Intermittency in premixed turbulent reacting flows

Peter E. Hamlington, Alexei Y. Poludnenko, and Elaine S. Oran

Citation: Physics of Fluids (1994-present) **24**, 075111 (2012); doi: 10.1063/1.4729615
View online: http://dx.doi.org/10.1063/1.4729615
View Table of Contents: http://scitation.aip.org/content/aip/journal/pof2/24/7?ver=pdfcov
Published by the AIP Publishing

Intermittency in premixed turbulent reacting flows

Peter E. Hamlington,[1,2] Alexei Y. Poludnenko,[1] and Elaine S. Oran[1]
[1]*Laboratories for Computational Physics and Fluid Dynamics, Naval Research Laboratory, Washington, DC 20375, USA*
[2]*Department of Aerospace Engineering Sciences, University of Colorado, Boulder, Colorado 80309, USA*

(Received 23 November 2011; accepted 8 May 2012; published online 25 July 2012)

Intermittency in premixed reacting flows is studied using numerical simulations of premixed flames at a range of turbulence intensities. The flames are modeled using a simplified reaction mechanism that represents a stoichiometric H_2-air mixture. Intermittency is associated with high probabilities of large fluctuations in flow quantities, and these fluctuations can have substantial effects on the evolution and structure of premixed flames. Intermittency is characterized here using probability density functions (pdfs) and moments of the local enstrophy, pseudo-dissipation rate (strain rate magnitude), and scalar (reactant mass fraction) dissipation rate. Simulations of homogeneous isotropic turbulence with a nonreacting passive scalar are also carried out in order to provide a baseline for analyzing the reacting flow results. In the reacting flow simulations, conditional analyses based on local, instantaneous values of the scalar are used to study variations in the pdfs, moments, and intermittency through the flame. For low intensities, pdfs of the local enstrophy vary substantially through the flame, with greater intermittency near the products. Changes in the pseudo-dissipation pdfs are, however, less pronounced. As the intensity increases, both the enstrophy and pseudo-dissipation pdfs become increasingly independent of position in the flame and are similar to results from the nonreacting simulations. The scalar dissipation intermittency is largest near the reactants and increases at all flame locations with increasing turbulence intensity. For low intensities and in the reaction zone, however, scalar dissipation pdfs approximately follow a Gaussian distribution, indicative of substantially reduced intermittency. Deviations from log-normality are observed in the pdfs of all quantities, even for intensities and flame locations characterized by strong intermittency. The implications of these results for the internal structure of the flame are discussed, and we also propose a connection between reacting flow intermittency and anisotropic vorticity suppression by the flame.
 [http://dx.doi.org/10.1063/1.4729615]

I. INTRODUCTION

A wide range of experimental[1–3] and numerical[4–9] studies have shown that local enstrophy, $\Omega = \omega_i' \omega_i'/2$, and energy dissipation rate, $\varepsilon = 2\nu S_{ij}' S_{ij}'$, fields in turbulent flows are intermittent, where ω_i' and S_{ij}' are the fluctuating vorticity and strain rate, respectively. Such intermittent fields are characterized by local, instantaneous values that can be considerably larger than the corresponding mean values. Moreover, these extreme values occur with substantially higher probability than would be expected from Gaussian statistics.[10,11] This results in probability density functions (pdfs) with stretched "tails" for large Ω and ε. Since ω_i' and S_{ij}' are given in terms of the fluctuating velocity, u_i', as

$$\omega_i' = \epsilon_{ijk} \frac{\partial u_k'}{\partial x_j}, \quad S_{ij}' = \frac{1}{2}\left(\frac{\partial u_i'}{\partial x_j} + \frac{\partial u_j'}{\partial x_i}\right), \tag{1}$$

where ϵ_{ijk} is the cyclic permutation tensor, the tails in the pdfs of Ω and ε are associated with the steepest velocity gradients in the flow. These extreme gradients are, in turn, connected to small-scale structures such as vortex filaments and dissipation sheets.[7,10,12,13] Similar small-scale intermittency has also been observed[3–7,9,14] in fields of the scalar dissipation rate, $\chi = 2D\chi_i'\chi_i'$, where D is the molecular diffusivity and χ_i' is the gradient of the scalar fluctuation, ϕ', given by

$$\chi_i' = \frac{\partial \phi'}{\partial x_i}. \tag{2}$$

Due to its prevalence in a wide range of flows for a variety of different quantities, small-scale intermittency appears to be a universal characteristic of turbulence.

Determining the detailed properties of turbulence intermittency—including its physical origins and its effect on inertial-range scaling exponents—is a major topic of research on nonreacting turbulence and passive scalar evolution (see Refs. 10 and 13 for reviews). Prior studies have shown that intermittency depends on both Reynolds, *Re*, and Schmidt, *Sc*, numbers,[8,9] and that it is strongest at small scales.[13] In homogeneous isotropic turbulence, Ω is more intermittent than ε,[2,8] and both Ω and ε are generally less intermittent than χ.[9] Intermittency in more complex flows is affected by additional factors, such as mean shear in jets and plumes,[1,3,14] mean scalar gradients in homogeneous flows,[4,5] wall distance in channel flows,[15,16] and viscoelasticity.[17] A number of studies[6,8,9,15,16,18] have also examined high-order moments of Ω, ε, and χ; these moments, which include the skewness and kurtosis (the third and fourth-order central moments, respectively), allow deviations from Gaussianity to be measured, and thus permit the degree of intermittency to be quantified.

While intermittency in nonreacting flows has received considerable attention, relatively little is known about intermittency in chemically reacting flows,[11,19] despite its importance for understanding the properties and interactions of turbulence and flames. In reacting flows, χ is associated with the chemical reaction rate[11,19–21] and the local flame width[22] (where ϕ' in Eq. (2) is a non-passive, non-conserved scalar in reacting flows). The statistical properties of χ, including pdfs and conditional averages, are also used in turbulent combustion models.[19,23] The turbulent vorticity and strain rate fields, whose local magnitudes are related to Ω and ε, are responsible for stretching, wrinkling, and broadening of premixed flames.[22] The intermittency associated with χ, Ω, and ε thus affects how often very thin or very broad flames occur, and how often the flame experiences very strong straining or rotation by turbulence (potentially resulting in the formation of large curvature and cusps[24]). Reacting flow intermittency also affects the likelihood of events such as extinction, auto- and re-ignition, and deflagration-to-detonation transitions (DDT).[25,26] These events, which can have considerable global consequences, may result from highly localized, very brief, and extreme (either very large or small) fluctuations in Ω, ε, and χ.

Several studies have examined the intermittency of χ in reacting flows, often with an emphasis on flame extinction and re-ignition. Karpetis and Barlow[27] found that χ in partially premixed, methane-air jet flames exhibits intermittency similar to that found in nonreacting flows. In particular, measured pdfs of the log variable $\ln(\chi)$ deviated from Gaussian distributions and had negative skewness. These deviations indicate that χ cannot be accurately described by a log-normal distribution (note that a variable, f, is considered to be log-normally distributed when $\ln(f)$ follows a Gaussian distribution). Similar deviations have been observed in non-premixed jet flames,[28,29] reacting shear layers,[30] and jet diffusion flames.[31,32] These deviations are significant, since the log-normal model has been proposed[33,34] as a description for intermittent turbulence and is used in turbulent combustion models.[35,36] Although Frisch[10] notes several problems with the log-normal model, and the negatively skewed pdfs are consistent with a number of prior nonreacting studies (e.g., Refs. 6 and 14), other studies of reacting flows[37,38] have indicated closer agreement with the log-normal model. Investigations of other configurations—including premixed reacting flows and flows with various fuel mixtures and different turbulence intensities—are needed in order to better understand the intermittency of Ω, ε, and χ in reacting flows, as well as to assess the accuracy of the log-normal model in more detail.

In the present study, we analyze intermittency in premixed reacting flows by examining pdfs and moments of Ω, the pseudo-dissipation rate, $\varepsilon^* = \varepsilon/\nu$, and χ using numerical simulations of statistically planar premixed flames at a range of turbulence intensities. A simplified reaction model

is used to represent a stoichiometric mixture of H_2 and air in the reactants.[39] Conditional statistics based on the local, instantaneous values of the reactant mass fraction, Y, are further used to examine variations in the pdfs and moments through the flame itself. These simulations have been used previously in a study of turbulence-flame interactions and first-order turbulence and flame statistics, including conditional averages and relative alignments of ω_i, S_{ij}, and χ_i.[22,40] The present study also substantially extends an earlier, preliminary study of intermittency in premixed reacting flows.[41] As a prelude to the reacting flow simulations, simulations of homogeneous isotropic turbulence with a nonreacting and conserved passive scalar are analyzed, and the results are then used as a baseline for comparisons with the reacting flow results. In all cases, pdfs from the simulation data are compared with log-normal distributions in order to assess the accuracy of the log-normal model in premixed reacting flows. We also consider the connection between turbulence-flame interactions and intermittency, as well as examine the effects of intermittency on distributions of the local flame width.

II. NUMERICAL SIMULATIONS

The present numerical simulations model premixed combustion in an unconfined domain by solving the compressible conservation equations for a reactive flow[24,42]

$$\frac{\partial \rho}{\partial t} + \frac{\partial (\rho u_i)}{\partial x_i} = 0, \tag{3}$$

$$\frac{\partial (\rho u_i)}{\partial t} + \frac{\partial (\rho u_i u_j)}{\partial x_j} + \frac{\partial P}{\partial x_i} = 0, \tag{4}$$

$$\frac{\partial E}{\partial t} + \frac{\partial [(E+P)u_j]}{\partial x_j} - \frac{\partial}{\partial x_j}\left(K \frac{\partial T}{\partial x_j}\right) = -\rho q \dot{\mathrm{w}}, \tag{5}$$

$$\frac{\partial (\rho Y)}{\partial t} + \frac{\partial (\rho Y u_j)}{\partial x_j} - \frac{\partial}{\partial x_j}\left(\rho D \frac{\partial Y}{\partial x_j}\right) = \rho \dot{\mathrm{w}}, \tag{6}$$

where u_i is the velocity, ρ is the density, P is the pressure, E is the energy density, T is the temperature, and q is the chemical energy release. The ideal gas equation of state is used for P, and the chemical reaction rate, $\dot{\mathrm{w}}$, is given by single-step, first-order Arrhenius kinetics[24,42] as

$$\dot{\mathrm{w}} = -A\rho Y \exp\left(-\frac{Q}{RT}\right), \tag{7}$$

where A is the pre-exponential factor, Q is the activation energy, and R is the universal gas constant. The coefficients of molecular diffusion, D, and thermal conduction, K, in Eqs. (5) and (6), respectively, are given by

$$D = D_0 \frac{T^n}{\rho}, \quad K = C_p \kappa_0 T^n, \tag{8}$$

where $C_p = \gamma R/M(\gamma - 1)$. The Lewis number, $Le = \kappa_0/D_0$, is unity for all simulations. Values of the model input parameters in Eqs. (3)–(8), summarized in Table I, represent a stoichiometric H_2-air mixture and are based on the reaction model of Gamezo *et al.*[39]

The simulations are carried out with the code Athena-RFX,[24,42] which uses a higher order, fully conservative Godunov-type method[43–45] to solve Eqs. (3)–(8). Turbulence is sustained in the simulations by adding large-scale perturbations to the velocity field.[24] These perturbations are isotropic and divergence free, and result in a constant energy injection rate per unit volume. Small-scale energy dissipation occurs through numerical viscosity, which allows an inertial range with Kolmogorov ($k^{-5/3}$, where k is the wavenumber) scaling to be extended to the scale of the laminar flame width, as shown in Fig. 1.[22,24,42] A previous study[24] has shown that this numerical method accurately captures both the flame and turbulence properties down to the scale of the laminar flame width.

Three different reacting flow simulations are examined, denoted F1, F3, and F5 in Table II and on the regime diagram in Fig. 2.[46] These simulations correspond to turbulence intensities I_T

TABLE I. Input model parameters and resulting laminar flame properties common to all reacting flow numerical simulations in this paper.[22,24]

T_0	293 K	Initial temperature
P_0	1.01×10^6 erg/cm^3	Initial pressure
ρ_0	8.73×10^{-4} g/cm^3	Initial density
γ	1.17	Adiabatic index
M	21 g/mol	Molecular weight
T_P	2135 K	Post-flame temperature
ρ_P	1.2×10^{-4} g/cm^3	Post-flame density
δ_L	0.032 cm	Laminar flame thermal width
S_L	302 cm/s	Laminar flame speed
A	6.85×10^{12} cm^3/(g s)	Pre-exponential factor
Q	46.37 RT$_0$	Activation energy
q	43.28 RT$_0$/M	Chemical energy release
κ_0	2.9×10^{-5} g/(s cm K^n)	Thermal conduction coefficient
D_0	2.9×10^{-5} g/(s cm K^n)	Molecular diffusion coefficient
n	0.7	Temperature exponent

$= U_l/S_L = 2.45$, 9.81, and 30.6, respectively, where U_l is the turbulent integral velocity in the unburned reactants and S_L is the laminar flame speed. The corresponding Damköhler numbers, $Da \equiv (l/U_l)/(l_F/S_L)$, are between 0.39 and 0.031, where l is the turbulence integral scale, $l_F = D(Y = 0.5)/S_L \approx 2\delta_L$, $\delta_L \equiv (T_b - T_u)/(dT/dx)_{L,\,max}$ is the thermal width of the laminar flame, and $l/\delta_L = 1.90$. The three simulations analyzed here have also been examined in a previous study[22] that included additional intermediate intensities $I_T = 4.90$ and 18.4 (denoted F2 and F4 in Ref. 22). The range of I_T spanned by the present simulations is, however, sufficient to determine trends in the statistics with I_T.

The length-to-width ratio of the computational domain for the simulations is L_x: $(L_y, L_z) = 16{:}1$, and the size of the grid is $N_x \times N_y \times N_z = 2048 \times 128 \times 128$. This grid size gives 16 computational

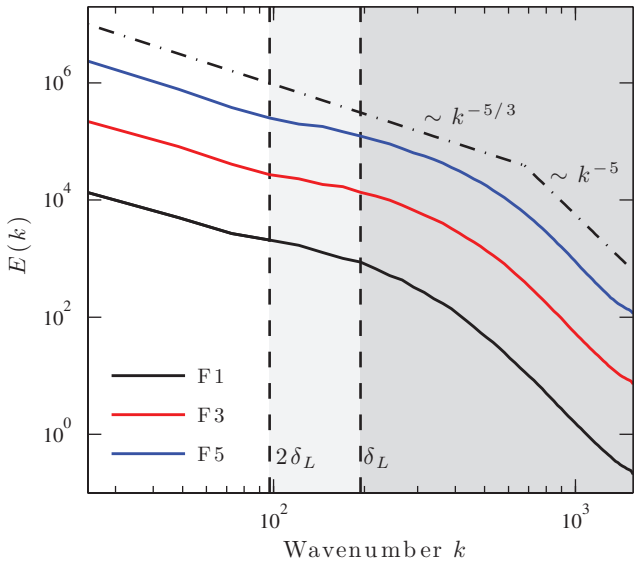

FIG. 1. Instantaneous kinetic energy spectra in the full computational domain immediately prior to ignition for F1, F3, and F5. Inertial ($k^{-5/3}$) and dissipation (k^{-5}) range scalings are shown by black dash-dot lines, and wavenumbers corresponding to δ_L and $2\delta_L$ are shown by vertical dashed lines, where δ_L is the laminar flame thermal width. Reproduced by permission from Hamlington *et al.*, Physics of Fluids **23**, 125111 (2011), where spectra for additional simulations F2 and F4 are also shown. Copyright © 2011 by American Institute of Physics.

TABLE II. Initial normalized turbulence intensity $I_T \equiv U_l/S_L$, Damköhler number, $Da = (l/U_l)/(l_F/S_L)$, and eddy-turnover time, $\tau_{ed} = L/U_L$, in the unburned mixture at ignition for the three reacting simulations, denoted F1, F3, and F5. The corresponding nonreacting simulations with the same I_T and τ_{ed} are denoted NR1, NR3, and NR5. The number of snapshots, N_t, is shown in the last column (with N_t for the nonreacting simulations shown in parentheses).

Simulation (nonreacting)	I_T	Da	$\tau_{ed}(s)$	N_t
F1 (NR1)	2.45	0.39	2.14×10^{-4}	540 (40)
F3 (NR3)	9.81	0.097	5.36×10^{-5}	630 (40)
F5 (NR5)	30.6	0.031	1.71×10^{-5}	600 (40)

cells per δ_L, which is sufficient to capture properties of the intermittency, as shown in Sec. V D through comparisons with results from an additional simulation of the intermediate intensity (F3) at resolution $N_x \times N_y \times N_z = 4096 \times 256 \times 256$ (32 cells per δ_L). Periodic boundary conditions are used in the spanwise (i.e., y and z) directions at all times, and in the x direction prior to ignition. After ignition, zero-order extrapolation boundary conditions are used on the x-boundaries in order to prevent pressure build-up inside the domain.

In all of the reacting flow simulations, nonreacting homogeneous isotropic turbulence is allowed to develop in the domain for $\sim 2\tau_{ed}$ prior to ignition, where $\tau_{ed} = L/U_L$ is the eddy-turnover time, $L = 0.259$ cm is the physical width of the computational domain, and U_L is the velocity at scale L. At $2\tau_{ed}$, a flame is initialized near the center of the x-axis using an exact laminar flame profile. Injection of random large-scale velocity perturbations is continued even after ignition, resulting in sustained turbulence-flame interactions. The time interval between regenerations of the random perturbation field is maintained at $\sim \tau_{ed}/40$ for all simulations.

The analysis of the simulations begins $2\tau_{ed}$ after ignition, and extends for up to another $1.5\tau_{ed}$ (i.e., up to $3.5\tau_{ed}$ after ignition). During the analysis phase, 20 snapshots are retained per τ_{ed} in order to obtain sufficient statistics. The statistics are further improved by non-deterministically restarting the simulations $2\tau_{ed}$ after ignition ($4\tau_{ed}$ after the start of the simulations). The non-deterministic nature of these restarts gives a different flow evolution in each realization from $2\tau_{ed}$ onwards. This procedure allows ensemble averaging of the statistics while also avoiding systematic temporal variations due to the gradual turbulent dissipative heating of the reactants. This heating is particularly pronounced for high I_T (resulting in a 4.9 K increase in reactant temperature per τ_{ed} for F5) and

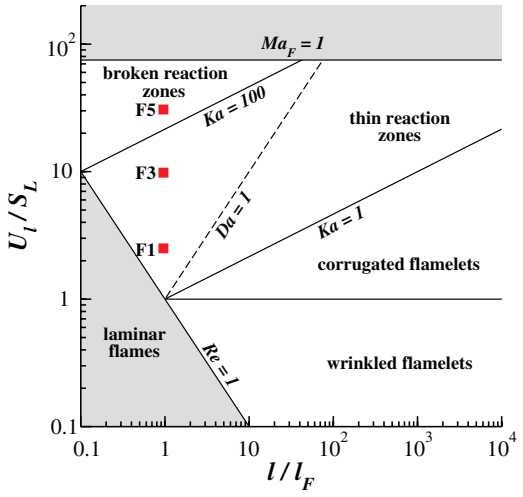

FIG. 2. Combustion regime diagram[46] showing the location of simulations F1, F3, and F5 (red squares). Here $Re = (lU_l)/(l_F S_L)$ is the Reynolds number, Ka is the Karlovitz number, and Ma_F is the turbulent Mach number in cold H_2-air fuel at atmospheric conditions. Reproduced by permission from Hamlington *et al.*, Physics of Fluids **23**, 125111 (2011), where the location of the additional simulations F2 and F4 is also shown. Copyright © 2011 by American Institute of Physics.

has been described in more detail in Refs. 22, 24, and 42. The non-deterministic restart procedure produces at least $N_t = 540$ temporal snapshots in the analysis of each I_T, as shown in Table II.

All derivatives used to obtain Ω, ε^*, and χ are calculated using fourth-order central differences, with fourth-order, one-sided differences along the edges of the simulation domain. Comparisons with second-order central differences indicate that the observed trends are independent of the accuracy with which the derivatives are calculated. For the reacting simulations, the scalar ϕ in Eq. (2) is set equal to the reactant mass fraction, Y, from Eq. (6), where $Y = 1$ in the reactants and $Y = 0$ in the products. The scalar gradient, χ_i', thus refers in the following to the reacting scalar gradient which is, in general, not passive, and χ denotes the corresponding reacting scalar dissipation.

Simulations of homogeneous isotropic turbulence and nonreacting passive scalar evolution in a fully periodic, cubic box are also carried out. The computational dimensions are $N_x \times N_y \times N_z = 128^3$, giving the same resolution as in the reacting simulations. Three intensities are examined, denoted NR1, NR3, and NR5, corresponding to the intensities used for F1, F3, and F5 (Table II). The nonreacting fluid properties are identical to those of the unburned reactants in the reacting flow simulations, and Eqs. (3)–(6) are again solved with D and K given by Eq. (8). In the nonreacting simulations, however, $\dot{w} = 0$, causing the scalar to be passive and conserved. To avoid confusion with the nonconserved Y in Eq. (6) and the corresponding reacting scalar gradient χ_i', the passive scalar in the nonreacting simulations is denoted ξ and its gradient $\zeta_i' = \partial\xi'/\partial x_i$. The nonreacting, passive scalar dissipation is then denoted $\zeta = 2D\zeta_i'\zeta_i'$. Analysis of the nonreacting simulations is carried out over a timespan equal to $4\tau_{ed}$, beginning $2\tau_{ed}$ after the start of the simulations, with 10 snapshots per τ_{ed} (giving $N_t = 40$, as shown in Table II). High statistical convergence is maintained since the entire 128^3 spatial domain can be used in the analysis at each time. This is in contrast to the reacting flow results which must be examined on a conditional basis, resulting in significantly fewer spatial points included in each of the conditional pdfs.

III. NONREACTING TURBULENT FLOWS

Before examining intermittency in the reacting flow simulations, we first analyze simulations of homogeneous isotropic turbulence with a nonreacting passive scalar. This preliminary analysis is important since the present simulations use numerical viscosity for energy dissipation, and the exact Reynolds number is thus difficult to establish. An effective Re based on the numerical viscosity could be defined, but this depends on the grid resolution and increases as the resolution increases. Since intermittency is Reynolds number dependent,[13] analysis of the reacting flow simulations thus requires us to first establish baseline intermittency properties using less complex nonreacting flow simulations. The same grid resolution is used in all simulations in order to achieve a consistent effective Reynolds number. Comparison of the reacting flow results with these baseline simulations allows variations in the statistics of Ω, ε^*, and χ with intensity and position in the flame to be understood. These preliminary simulations also validate the numerical method by showing that the measured pdfs and moments of Ω, ε^*, and ζ are consistent with prior results from direct numerical simulations (DNS) (Refs. 4–6 and 9) and experiments[1] of homogeneous isotropic turbulence and passive scalar evolution. It should also be noted that intermittency in nonreacting flows has been studied previously using simulations that follow the approach used in implicit large-eddy simulation (ILES),[47,48] where physical viscosity is not explicitly included and numerical viscosity is used to dissipate energy at the smallest scales. In particular, Benzi *et al.*[49] and Porter *et al.*[50] have studied the scaling of higher order structure functions and intermittency, showing good agreement with results from prior DNS studies. Resolution and Reynolds number effects in the reacting flow simulations are further discussed in Sec. V D using a higher resolution simulation of F3.

A. Pdfs of u_x and ξ

Figure 3 shows pdfs of the velocity component u_x and the passive, conserved scalar ξ for NR1, NR3, and NR5. The arguments of the pdfs are normalized using the mean, $\mu_f \equiv \langle f \rangle$, and the standard deviation, $\sigma_f \equiv \langle (f - \mu_f)^2 \rangle^{1/2}$, where f represents a flow variable and $\langle \cdot \rangle$ denotes a spatial average over the full simulation domain. The averages are calculated separately at each temporal snapshot,

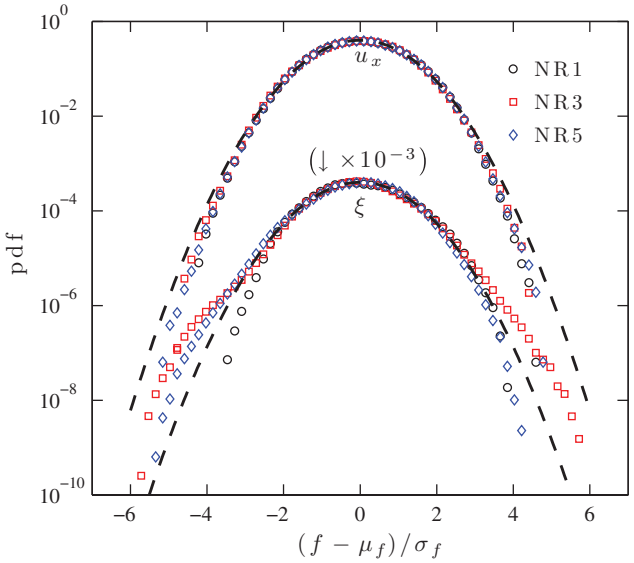

FIG. 3. Pdfs of velocity, $(u_x - \mu_u)/\sigma_u$, and passive scalar, $(\xi - \mu_\xi)/\sigma_\xi$, for NR1, NR3, and NR5. Pdfs for ξ are shifted down by three decades for clarity. Dashed black lines show Gaussian distributions.

and the resulting data are included in a single, effectively time-averaged, pdf. Note that since $\mu_u \approx 0$ for the nonreacting data, u_x is approximately equal to its corresponding fluctuating quantity, u_x'. The mean of ξ is close to 0.5, and Fig. 3 shows pdfs of the fluctuating variable $\xi' = \xi - \mu_\xi$. Each pdf (including the conditional pdfs examined in Sec. IV) is normalized such that the integral of the pdf over all values of its argument is unity.

Figure 3 shows that pdfs of u_x approximately follow a Gaussian distribution for all I_T, with slight departures from Gaussianity in both the left and right tails. Similar results are observed for ξ in Fig. 3, again with deviations from the Gaussian distribution in the tails. The approximate Gaussianity of both u_x and ξ for all I_T in Fig. 3, including the departures from Gaussianity for large and small values, is consistent with prior studies[4,5] of homogeneous isotropic turbulence and nonreacting passive scalar evolution.

B. Pdfs of Ω, ε*, and ζ

Pdfs of Ω, ε^*, and ζ normalized by their respective mean values are shown for the nonreacting simulations in Fig. 4. Since the flow is homogeneous, the average gradients $\partial\langle u_i\rangle/\partial x_j$ and $\partial\langle\xi\rangle/\partial x_i$

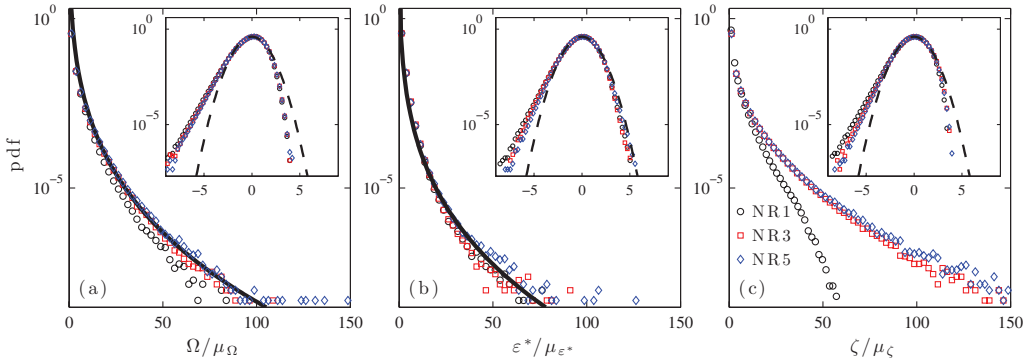

FIG. 4. Pdfs of (a) Ω/μ_Ω, (b) $\varepsilon^*/\mu_{\varepsilon^*}$, and (c) ζ/μ_ζ for NR1, NR3, and NR5. Stretched exponentials $d_1 \exp[-d_2(f/\mu_f)^{0.25}]$ are shown by black lines in (a) and (b). Insets show pdfs of (a) $[\ln(\Omega) - \tilde{\mu}_\Omega]/\tilde{\sigma}_\Omega$, (b) $[\ln(\varepsilon^*) - \tilde{\mu}_{\varepsilon^*}]/\tilde{\sigma}_{\varepsilon^*}$, and (c) $[\ln(\zeta) - \tilde{\mu}_\zeta]/\tilde{\sigma}_\zeta$; dashed black lines in insets show Gaussian distributions of log variables, corresponding to the log-normal model.

are approximately zero, and ω_i', S_{ij}', and ζ_i' in Eqs. (1) and (2) can be obtained without explicitly subtracting mean values. For all quantities, Fig. 4 shows that the pdfs have stretched tails for large values of Ω, ε^*, and ζ, indicative of intermittent distributions. The pdfs of Ω and ε^* are similar to those observed previously in studies of homogeneous isotropic turbulence.[2,8,9] As noted before, the pdfs of Ω are more strongly stretched at high values than those for ε^*. This difference may disappear for high Re at very large values of Ω/μ_Ω and $\varepsilon^*/\mu_{\varepsilon^*}$,[8] but investigating this point further would require much higher numerical resolutions than used in the present simulations.

Consistent with prior studies,[2,8] the pdfs of Ω and ε^* in Figs. 4(a) and 4(b) can be described using stretched exponentials of the form $d_1 \exp[-d_2(f/\mu_f)^{d_3}]$, where the d_i are obtained from fits to the data.[8] Here we use $d_3 = 0.25$, which was found by Donzis *et al.*[8] to be the limit value of d_3 as the resolution was increased in simulations of homogeneous isotropic turbulence. The pdfs in Figs. 4(a) and 4(b) are reasonably approximated by stretched exponentials with $[d_1, d_2] = [3.3 \times 10^4, 9.4]$ for Ω/μ_ω and $[d_1, d_2] = [3.3 \times 10^3, 9.3]$ for ε^*/μ_S. Depending on the Reynolds number and simulation resolution, Donzis *et al.*[8] measured $d_2 \approx 5$–7 for Ω and $d_2 \approx 7$–11 for ε, which are relatively close to the current measured values.

The pdfs of ζ in Fig. 4(c) are also stretched for large values of ζ and, for sufficiently high I_T, show stronger intermittency than the Ω and ε^* pdfs. The increased intermittency of ζ compared to Ω and ε^* is in agreement with prior studies of passive scalar evolution.[9] The stretching of the ζ pdfs increases with I_T, as shown by the significantly more prominent tail for NR5 than NR1. This variation is due to changes in the competing processes of turbulent production of ζ by S_{ij} and destruction by molecular diffusion. As I_T increases, the turbulence becomes more effective at creating large ζ, resulting in the increasingly stretched tails for large I_T shown in Fig. 4(c).

The insets in Fig. 4 compare pdfs of $\ln(\Omega)$, $\ln(\varepsilon^*)$, and $\ln(\zeta)$ with Gaussian distributions given by $\exp[-(\ln f - \tilde{\mu}_f)^2/2\tilde{\sigma}_f^2]$, where the tilde[3] denotes statistics of the log variable $\ln(f)$. For each quantity, the pdfs are above the Gaussian distributions at the left tails, and below the Gaussian distributions at the right tails, resulting in negative skewness. Comparison of the insets in Figs. 4(a) and 4(b) shows that pdfs of $\ln(\varepsilon^*)$ match the Gaussians more closely than pdfs of $\ln(\Omega)$. The deviation of the $\ln(\zeta)$ pdfs from Gaussian distributions, and in particular the negative skewness, is similar to that observed previously for isotropic[6] and sheared[4] turbulence, as well as for axisymmetric turbulent plumes.[3] The inset of Fig. 4(c) does show, however, that in contrast to the substantially different pdfs of ζ, the pdfs of $\ln(\zeta)$ are very similar to each other for all values of I_T.

C. Central moments

Deviations of the Ω, ε^*, and ζ pdfs in Fig. 4 from Gaussian and log-normal distributions can be measured quantitatively using the normalized standard deviation, $\sigma_f' \equiv \sigma_f/\mu_f$, skewness, $s_f \equiv \langle(f-\mu_f)^3\rangle/\sigma_f^3$, and kurtosis, $k_f \equiv \langle(f-\mu_f)^4\rangle/\sigma_f^4$,[13,51] where f is again a flow variable. These quantities are the second through fourth normalized central moments of f, and for a Gaussian pdf, $s_f = 0$ and $k_f = 3$. Similarly, $\tilde{s}_f = 0$ and $\tilde{k}_f = 3$ when f is log-normally distributed, where the tilde denotes statistics of the log variable $\ln(f)$. The value of σ_f' can be compared with results from prior studies of intermittency in homogeneous isotropic turbulence and passive scalar evolution (e.g., Donzis *et al.*[8,9]).

Table III shows central moments of Ω, ε^*, and ζ for NR1, NR3, and NR5, including moments of the corresponding log-variables. The moments are measured separately in each snapshot, and then averaged over all snapshots to obtain the values in Table III. Moments for both Ω and ε^* show departures from Gaussian values. For Ω, s_Ω increases from 4.5 for NR1 to 5.4 for NR5, while k_Ω increases from 44 to 68 over the same range of I_T. These moments indicate a weak increase in the intermittency of Ω with I_T, consistent with the pdfs in Fig. 4(a). Moments for ε^* suggest slightly weaker intermittency, again consistent with Fig. 4(b), with s_{ε^*} varying with I_T from 3.6 to 4.1, and k_{ε^*} varying from 34 to 53. Although the moments of $\ln(\Omega)$ and $\ln(\varepsilon^*)$ in Table III indicate that the log-normal model provides a reasonably accurate description of the measured pdfs, negative values of the log-skewness, and positive values of the excess log-kurtosis (i.e., $\tilde{k}_f - 3$) persist for both Ω and ε^* at all I_T.

TABLE III. Second through fourth central moments of Ω, ε^*, and ζ for nonreacting simulations NR1, NR3, and NR5. The normalized standard deviation is given by $\sigma'_f = \sigma_f/\mu_f$, the skewness is given by $s_f = \langle (f-\mu_f)^3\rangle/\sigma_f^3$, and the kurtosis is given by $k_f = \langle (f-\mu_f)^4\rangle/\sigma_f^4$. Values in parentheses are moments of log variables $\ln(f)$.

	NR1	NR2	NR3
σ'_Ω	1.41 (0.0567)	1.56 (0.0528)	1.62 (0.0497)
s_Ω	4.49 (−0.490)	5.19 (−0.431)	5.44 (−0.413)
k_Ω	44.4 (3.48)	57.9 (3.37)	68.0 (3.33)
σ'_{ε^*}	1.05 (0.0413)	1.08 (0.0375)	1.06 (0.0327)
s_{ε^*}	3.59 (−0.277)	3.60 (−0.274)	4.07 (−0.191)
k_{ε^*}	33.5 (3.29)	33.7 (3.22)	53.3 (3.11)
σ'_ζ	1.62 (−0.305)	2.17 (−0.623)	2.22 (−0.358)
s_ζ	4.80 (−0.365)	7.28 (−0.215)	7.81 (−0.214)
k_ζ	42.9 (3.31)	99.8 (3.13)	126 (3.06)

Table III shows that the moments of Ω and ε^* vary relatively weakly with I_T. These variations are likely due to changes in the effective Reynolds number with I_T. Similar variations in the moments of Ω and ε^* with Taylor microscale Reynolds number, Re_λ, have been observed in prior studies[6,8] of homogeneous isotropic turbulence. The moments in Table III are approximately consistent with those found by Vedula *et al.*[6] for Re_λ between 38 and 90. For high I_T, the turbulence also becomes weakly compressible, giving $S'_{kk} \neq 0$ (the turbulent Mach number is only 0.03 for F1, but increases to 0.4 for F5). This could have an additional effect, in particular, on the statistics of ε^*, since ε^* is directly related to S'_{ij}.

Consistent with prior studies,[6,9] the moments of ζ in Table III show that ζ is generally more intermittent than both Ω and ε^*, particularly for high I_T. Both s_ζ and k_ζ increase substantially with I_T, reflecting changes in the advection-diffusion balance governing the scalar dynamics. These variations may also be due to changes in the effective Reynolds and Schmidt numbers with I_T. Previous studies[6] of passive scalar evolution have shown that the intermittency associated with ζ depends on both of these parameters.

Figures 3 and 4 and Table III indicate that, for these nonreacting turbulent flows, the numerical method outlined in Sec. II produces homogeneous isotropic turbulence and passive scalar statistics consistent with prior numerical and experimental studies. In particular, the pdfs of Ω and ε^* in Figs. 4(a) and 4(b) show that many subtle turbulence properties observed in previous studies can be reproduced by solving Eqs. (3)–(6) using ILES. While there are small quantitative differences from prior DNS and experimental studies (for example, in the coefficients of the stretched exponential fits in Fig. 4), the results are qualitatively the same whether energy dissipation occurs through physical or numerical viscosity. This is consistent with the findings of Benzi *et al.*,[49] who note that the effects of numerical dissipation can be understood in terms of an effective viscosity that gives a corresponding effective Reynolds number. This is discussed in more detail in Sec. V D in the context of reacting flows. The results shown in Figs. 3 and 4 and in Table III are next used for comparisons with results in premixed reacting flows.

IV. PREMIXED REACTING FLOWS

Premixed reacting flow simulations have been carried out at the same resolutions, and hence the same effective Reynolds numbers, as the nonreacting simulations described above. For fluid dynamic quantities (i.e., u_x, Ω, and ε^*), this allows direct comparisons of the reacting flow pdfs and moments with those from the nonreacting flows. Such direct comparisons are, however, not possible for ζ and χ (the nonreacting and reacting scalar dissipation rates, respectively), since the nonreacting scalar, ξ, is passive and conserved, while the reacting scalar, Y, is not. These two scalars thus represent distinctly different quantities. Although direct quantitative comparisons of the ζ and

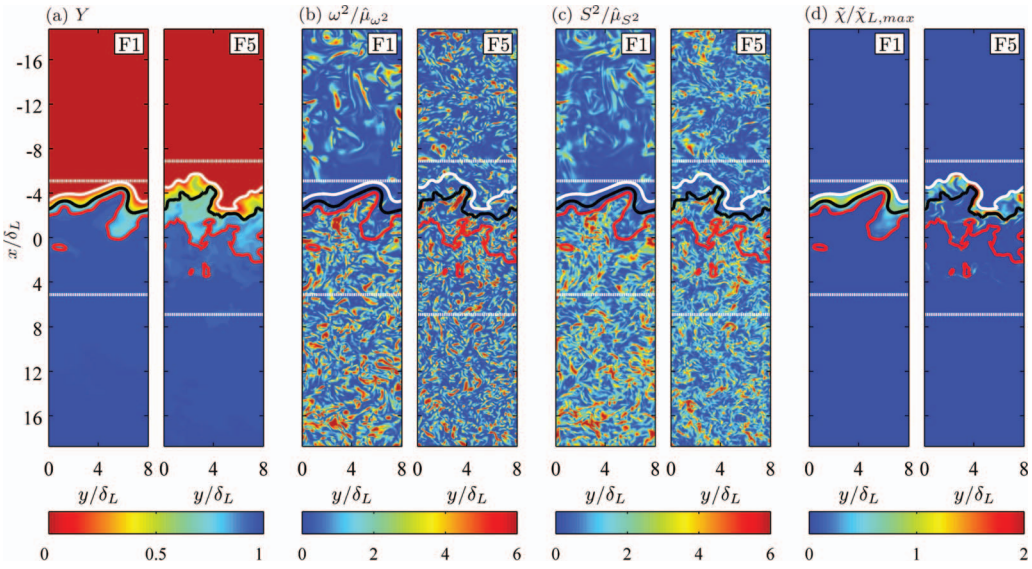

FIG. 5. Instantaneous fields of (a) Y, (b) $\omega^2/\hat{\mu}_{\omega^2}$, (c) $S^2/\hat{\mu}_{S^2}$, and (d) $\tilde{\chi}/\tilde{\chi}_{L,max}$ along the center of z-axis for F1 (left panels) and F5 (right panels), where $\hat{\mu}_{\omega^2}$ and $\hat{\mu}_{S^2}$ denote averages from the nonreacting simulations and $\tilde{\chi}_{L,max}$ is the maximum value of $\tilde{\chi}$ in the laminar flame. White dashed lines show bounds of flame brush beyond which $Y < 0.05$ (top line) and $Y > 0.95$ (bottom line) at all points. Solid white, black, and red contours correspond to $Y = 0.1$, 0.6, and 0.9, respectively.

χ statistics are difficult, we nevertheless use the nonreacting results in the following as a baseline for understanding variations in the statistics of χ with I_T and location in the flame.

A. Instantaneous fields

Figure 5 shows instantaneous fields of Y, $\omega^2 = \omega_i\omega_i$, $S^2 = S_{ij}S_{ji}$, and $\tilde{\chi} = \chi_i\chi_i$ for the reacting flow simulations F1 and F5, where ω_i, S_{ij}, and $\chi_i = \partial Y/\partial x_i$ are the total vorticity, strain rate, and scalar gradient, respectively (these quantities are closely connected to Ω, ε^*, and χ, respectively). Issues associated with defining the fluctuating variables ω_i', S_{ij}', and χ_i' necessary to obtain Ω, ε^*, and χ in reacting flows are discussed in more detail in Secs. IV B and IV C. For the H_2-air reaction-diffusion model used here, the $Y = 0.6$ isosurface in Fig. 5(a) approximately separates the preheat ($Y > 0.6$) and reaction ($Y < 0.6$) zones.[24] The bounds of the flame brush are defined as the maximum (minimum) x locations below (above) which $Y < 0.05$ ($Y > 0.95$) at all points. The contours of Y in Fig. 5(a) show that the flame is more wrinkled near the reactants than the products, and that the degree of wrinkling throughout the flame increases with I_T. The separation between the $Y = 0.6$ and $Y = 0.9$ contours increases from F1 to F5, which suggests that the width of the preheat zone increases with I_T. The width of the reaction zone (given by the separation between the $Y = 0.1$ and $Y = 0.6$ contours) remains relatively unchanged as I_T increases, as discussed in more detail in previous studies.[22,24,42]

Figures 5(b) and 5(c) show that ω^2 and S^2 are both suppressed by the flame for F1, but as I_T increases, this suppression becomes substantially less pronounced. For both F1 and F5, the ω^2 and S^2 fields are characterized by localized regions of large ω^2 and S^2, and values in these regions are higher compared to the mean for ω^2 than S^2. Figure 5(d) shows that $\tilde{\chi}$ is zero in the reactants and products, since Y is constant in these regions. Within the flame brush, however, there are thin regions of large $\tilde{\chi}$ inside the reaction zone ($Y < 0.6$), while $\tilde{\chi}$ is substantially weaker in the preheat zone ($Y > 0.6$), particularly for F5.

B. Conditional pdfs of u_x

Quantitative analysis of the reacting flow fields in Fig. 5 is complicated by the substantial spatial inhomogeneity of the flame brush. Examining intermittency at different locations within the

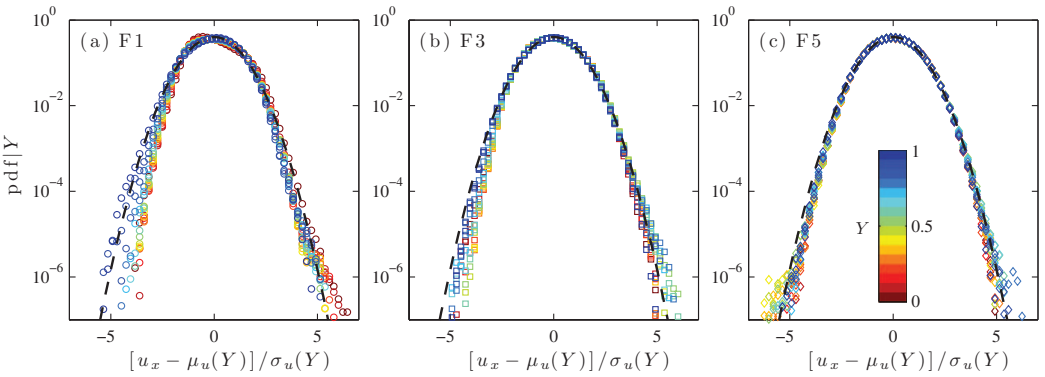

FIG. 6. Conditional pdfs of $[u_x - \mu_u(Y)]/\sigma_u(Y)$ for (a) F1, (b) F3, and (c) F5, where $\mu_u(Y)$ and $\sigma_u(Y)$ are conditional statistics based on Y. Dashed black lines show Gaussian distributions. Colorbar for all pdfs is shown in (c).

flame thus requires calculation of conditional pdfs based on the local, instantaneous values of Y. Both μ and σ must also be calculated by conditional averaging, where $\mu_f(Y) \equiv \langle f|Y\rangle$, $\sigma_f(Y) \equiv \langle [f - \mu_f(Y)]^2|Y\rangle^{1/2}$, and $\langle \cdot|Y\rangle$ denotes a conditional average over the entire flame brush. In the following analysis, 16 values of Y between 0 and 1 are used to construct the conditional pdfs. The analysis does not, however, include points where $Y < 0.01$ or $Y > 0.99$, since $Y \approx 0$ and $Y \approx 1$ correspond to completely burned and unburned mixtures, respectively.

Figure 6 shows conditional pdfs of u_x for F1–F5. These pdfs can be compared with the corresponding nonreacting pdfs in Fig. 3. The conditional pdfs approximately follow Gaussian distributions at all Y, although for low I_T there is a slight shift in the pdfs with location in the flame. In particular, for $Y \to 0$ (near the products), the right tails of the pdfs follow the Gaussian distribution more closely than the left tails. This relatively weak asymmetry becomes less pronounced, however, for $Y \to 1$ (near the reactants) and for higher I_T, as shown for F3 and F5 in Figs. 6(b) and 6(c).

The quantity $[u_x - \mu_u(Y)]$ in Fig. 6 can be viewed as the fluctuating u_x, calculated on a conditional basis. Fluctuating quantities are typically formed by subtracting spatial averages that have been calculated over homogeneous directions in the flow (for example, all three directions in homogeneous isotropic turbulence or planes parallel to walls in fully developed wall-bounded flows). These spatial averages are often combined with temporal or ensemble averages before calculating fluctuating variables. In reacting flows, however, calculation of fluctuating variables is complicated by the inhomogeneity associated with wrinkled flame surfaces (i.e., the isosurfaces of Y shown in Fig. 5(a)). Since the inhomogeneity in ρ, T, and other quantities is most closely associated with changes across these surfaces, all averages used to obtain fluctuating variables in the reacting simulations are calculated on a conditional basis with respect to Y. This is equivalent to assuming that, within the flame brush, the flow is essentially homogeneous along surfaces of constant Y. In Sec. IV C, conditional averaging at each Y is used to obtain the fluctuating variables ω_i', S_{ij}', and χ_i', which are then used to calculate statistics of Ω, ε^*, and χ.

C. Conditional pdfs of Ω, ε*, and χ

Figures 7–9 show that, in premixed reacting flows, there are variations in the conditional pdfs of Ω, ε^*, and χ as a function of both I_T and Y. As noted in Sec. IV B, these quantities are calculated using the conditional, fluctuating variables $\omega_i' = \omega_i - \langle \omega_i|Y\rangle$, $S_{ij}' = S_{ij} - \langle S_{ij}|Y\rangle$, and $\chi_i' = \chi_i - \langle \chi_i|Y\rangle$. For all I_T and Y, Figs. 7 and 8 show that Ω and ε^* are intermittent and have stretched tails. For Ω, however, the intermittency is significantly stronger near the products than the reactants. Near the reactants, the pdfs of Ω are similar to the stretched exponential curve-fit obtained from the nonreacting pdfs in Fig. 4(a). As I_T increases, variations in the Ω pdfs through the flame become weaker (Fig. 7(c)), and they approach the nonreactive behavior.

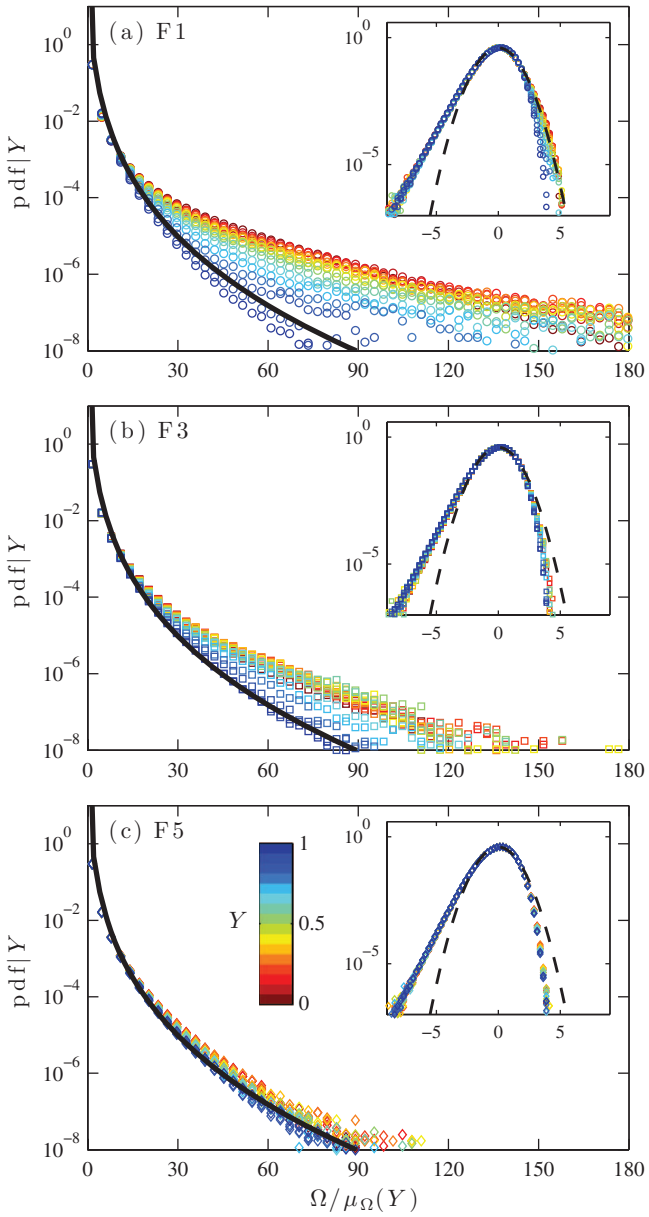

FIG. 7. Conditional pdfs of $\Omega/\mu_\Omega(Y)$ for (a) F1, (b) F3, and (c) F5. Stretched exponentials $d_1 \exp[-d_2(\Omega/\mu_\Omega)^{0.25}]$ from Fig. 4(a) are shown by black lines. Insets show pdfs of $[\ln(\Omega)-\tilde{\mu}_\Omega(Y)]/\tilde{\sigma}_\Omega(Y)$; dashed black lines show Gaussian distributions (corresponding to log-normal distributions of Ω).

As with the nonreacting results in Fig. 4, the pdfs of ε^* in Fig. 8 are less intermittent than pdfs of Ω, and there are also comparatively weaker variations in the ε^* pdfs through the flame. At the same time, as with the Ω pdfs in Fig. 7, the pdfs of ε^* are slightly more intermittent near the products at low I_T, and the variations in the pdfs through the flame become less pronounced as I_T increases. Furthermore, the pdfs of ε^* near the reactants are also in good agreement with the stretched exponential curve fit from the nonreacting results in Fig. 4(b).

The conditional pdfs of χ in Fig. 9 show that the probability of obtaining large $\chi/\mu_\chi(Y)$ increases with increasing I_T. There are also substantial variations in the pdfs through the flame itself. In particular, large $\chi/\mu_\chi(Y)$ is found primarily near the reactants ($Y \to 1$), with relatively low probability of large $\chi/\mu_\chi(Y)$ in the reaction zone. The pdfs of χ in the reaction zone for the

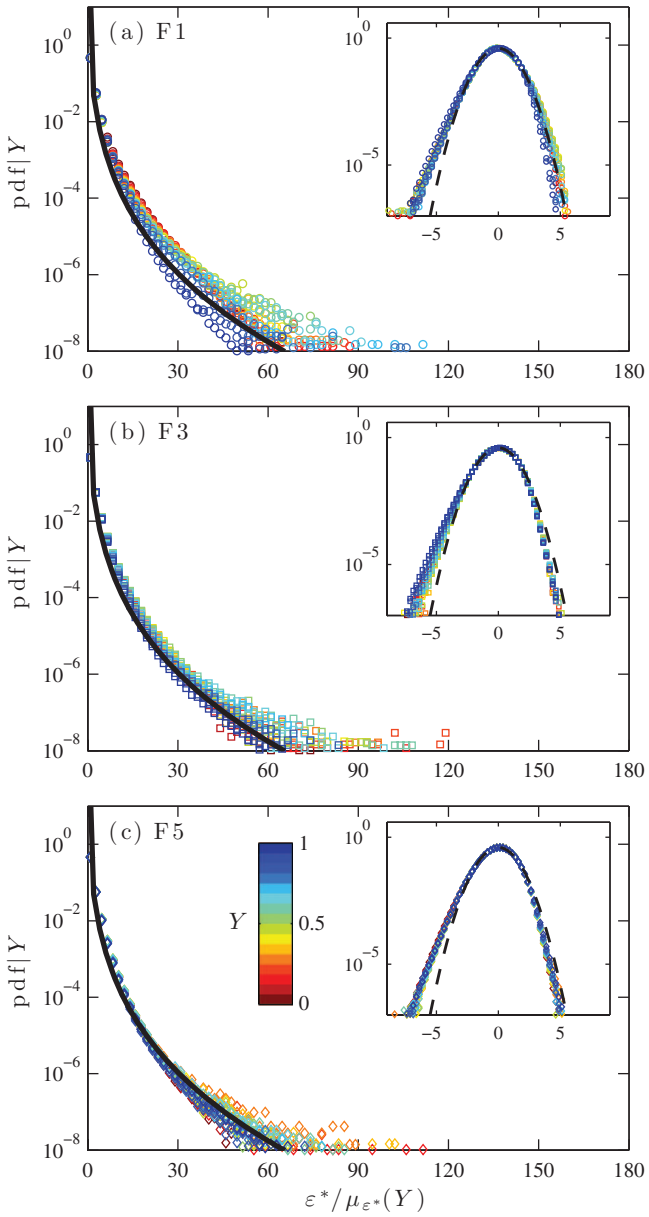

FIG. 8. Conditional pdfs of $\varepsilon^*/\mu_{\varepsilon^*}(Y)$ for (a) F1, (b) F3, and (c) F5. Stretched exponentials $d_1 \exp[-d_2(\varepsilon^*/\mu_{\varepsilon^*})^{0.25}]$ from Fig. 4(b) are shown by black lines. Insets show pdfs of $[\ln(\varepsilon^*)-\tilde{\mu}_{\varepsilon^*}(Y)]/\tilde{\sigma}_{\varepsilon^*}(Y)$; dashed black lines show Gaussian distributions (corresponding to log-normal distributions of ε^*).

smallest I_T (F1) are well-approximated by Gaussian distributions, indicating substantially reduced intermittency. For large I_T in Fig. 9, however, pdfs even on the product side of the flame show some degree of stretching and departures from Gaussianity.

D. Distributions of log variables

The pdfs of $\ln(\Omega)$ and $\ln(\varepsilon^*)$, which are compared with Gaussian distributions in the insets of Figs. 7 and 8, indicate that the log-normal distribution provides only an approximate model for intermittency of Ω and ε^* in reacting flows, consistent with the nonreacting results in Figs. 4(a) and 4(b). There are some changes in these pdfs with Y, particularly in the right tails for small

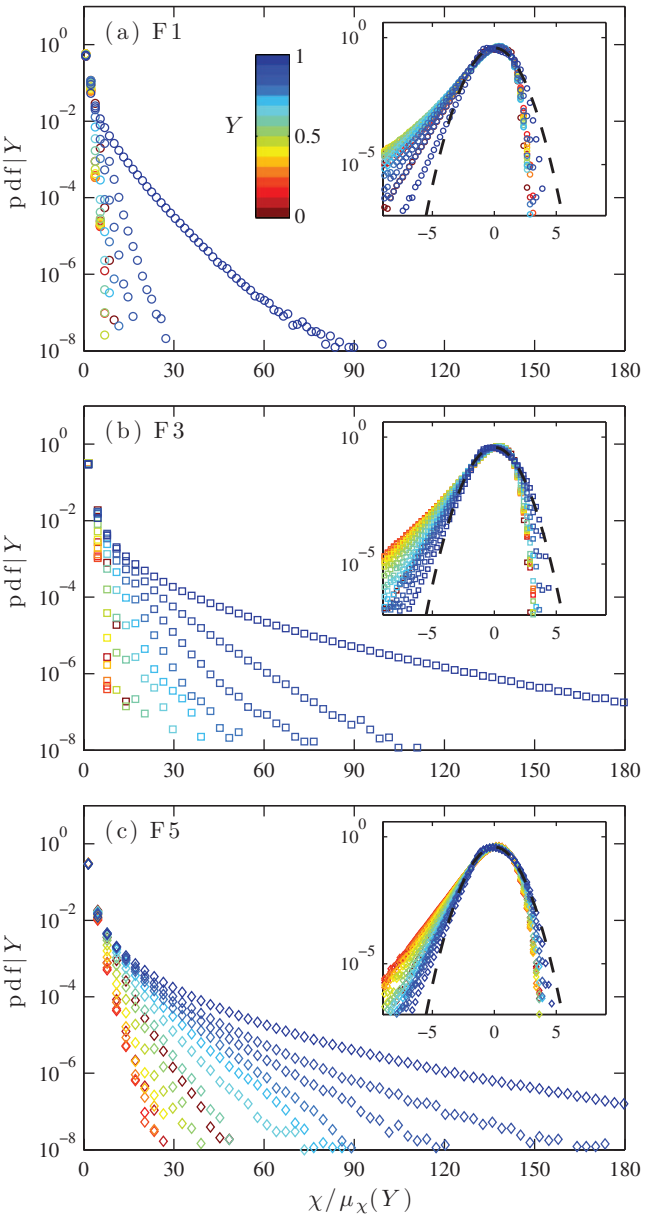

FIG. 9. Conditional pdfs of $\chi/\mu_\chi(Y)$ for (a) F1, (b) F3, and (c) F5. Insets show conditional pdfs of $[\ln(\chi) - \tilde{\mu}_\chi(Y)]/\tilde{\sigma}_\chi(Y)$; dashed black lines show Gaussian distributions (corresponding to log-normal distributions of χ).

I_T, although the variations are relatively weak. The most pronounced changes with I_T and Y are observed for $\ln(\chi)$ (insets of Fig. 9). For all I_T, the right tails of these pdfs are below the Gaussian distribution. The left tails become increasingly far from the Gaussian distribution as $Y \to 0$, resulting in negative skewness. Figure 9 also shows that variations in the pdfs with Y become smaller for high I_T.

The pdfs of $\ln(\chi)$ for small I_T and small Y (inset of Fig. 9(a)) are consistent with a Gaussian distribution for χ. In log coordinates, such a distribution has a stretched and slightly curved left tail, in agreement with the observed results. As I_T increases, this Gaussianity is lost and the left tails increasingly conform to the nonreacting distribution shown in the inset of Fig. 4(c). It is emphasized, however, that Fig. 9 indicates that the log-normal distribution is, in general, not an accurate model for χ pdfs in the present premixed flames. For all I_T, the pdfs of $\ln(\chi)$ are characterized by negative

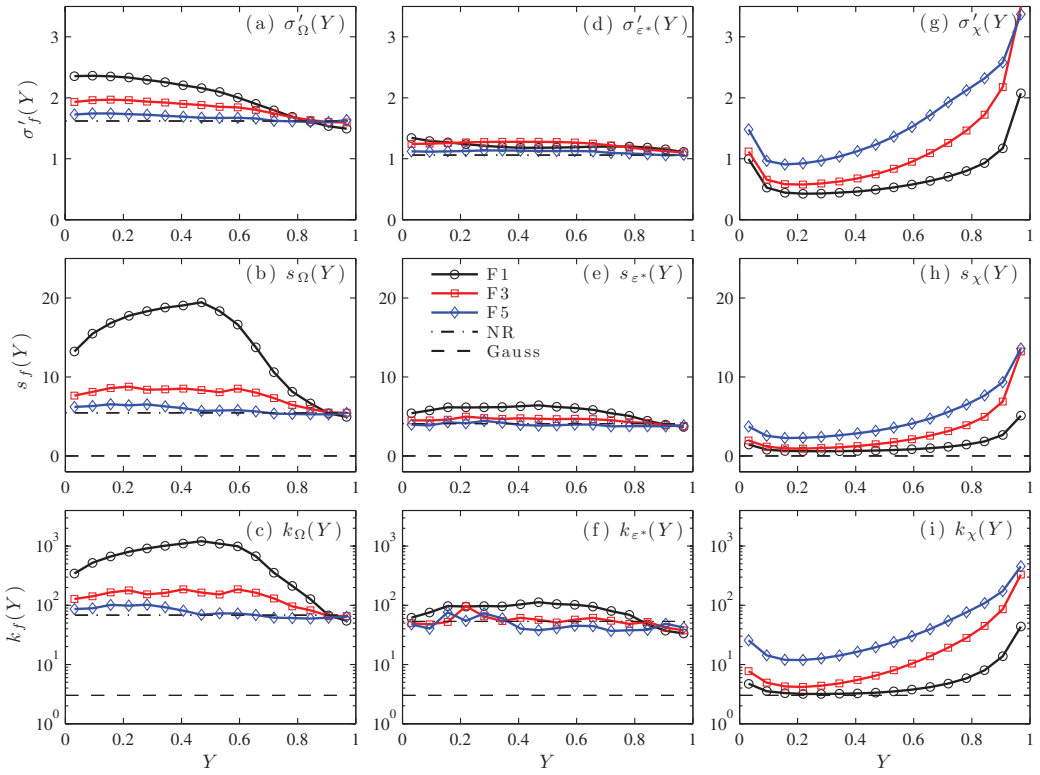

FIG. 10. Second through fourth conditional central moments of Ω (a)–(c), ε^* (d)–(f), and χ (g)–(i) as a function of Y for F1, F3, and F5. Results from nonreacting simulations (NR5, see Table III) are shown by dash-dot lines, and Gaussian values of 0 (for skewness, s_f) and 3 (for kurtosis, k_f) are shown by dashed lines. Legend is in the center panel (e).

skewness and departures from Gaussianity (corresponding to departures of χ from log-normality), consistent with previous observations in both nonreacting[3,4,6,14] and reacting[27–32] flows.

E. Conditional central moments

As noted in Sec. III C, the normalized standard deviation, σ'_f, skewness, s_f, and kurtosis, k_f, provide quantitative measures by which departures from Gaussianity can be measured. For the reacting flow simulations, we consider conditional values of these moments given by $\sigma'_f(Y) \equiv \sigma_f(Y)/\mu_f(Y)$, $s_f(Y) \equiv \langle[f-\mu_f(Y)]^3|Y\rangle/\sigma_f(Y)^3$, and $k_f(Y) \equiv \langle[f-\mu_f(Y)]^4|Y\rangle/\sigma_f(Y)^4$.

Figure 10 shows conditional moments of Ω, ε^*, and χ as a function of both I_T and Y. As in Table III, the moments are calculated separately in each snapshot and then averaged over all snapshots to obtain the values shown in Fig. 10. The moments of Ω in Figs. 10(a)–10(c) depart substantially from the Gaussian values at all Y, which is indicative of strong intermittency. The moments are, however, similar to the nonreacting values in Table III for $Y \to 1$ at small I_T, and at essentially all Y for higher I_T. This confirms the observation from Fig. 7 that the Ω pdfs are more stretched and intermittent for small Y and low I_T, but that the pdfs become increasingly similar to their nonreacting forms with increasing Y (towards the reactants) and I_T.

The conditional moments of ε^* in Figs. 10(d)–10(f) show weaker variations with both Y and I_T. The moments are similar to the nonreacting values from Table III for all Y at high I_T. A slight increase in $s_{\varepsilon^*}(Y)$ and $k_{\varepsilon^*}(Y)$ is seen for low I_T at $Y \approx 0.5$ in Figs. 10(e) and 10(f), but the change is relatively weak, particularly when compared to the large variations in $s_\Omega(Y)$ and $k_\Omega(Y)$ with both Y and I_T shown in Figs. 10(b) and 10(c).

The greatest variations with Y and I_T are seen in the conditional moments of χ in Figs. 10(g)–10(i). For each I_T, the moments are largest in the preheat zone, and the moments increase at all Y with

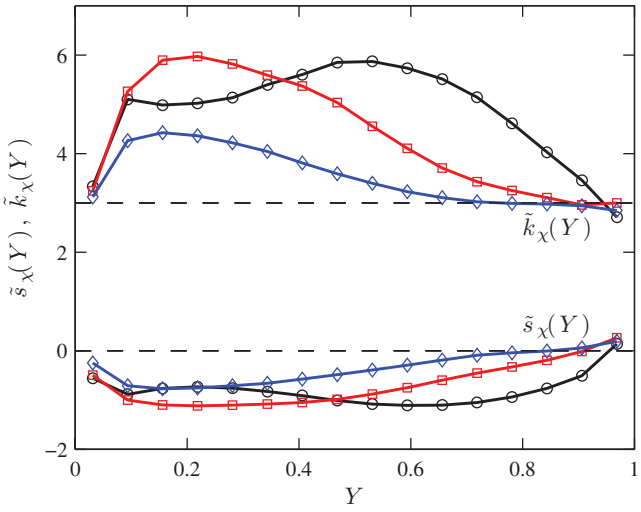

FIG. 11. Conditional skewness, $\tilde{s}_\chi(Y)$, and kurtosis, $\tilde{k}_\chi(Y)$, of $\ln(\chi)$ for F1, F3, and F5. Line styles are the same as in Fig. 10 and Gaussian values $\tilde{s}_\chi(Y) = 0$ and $\tilde{k}_\chi(Y) = 3$ (corresponding to log-normal distributions of χ) are shown by dashed lines.

increasing I_T. This suggests that the strongest intermittency in χ is observed for high I_T and in the preheat zone. For the lowest I_T examined here (F1), however, the third and fourth moments approach the Gaussian values $s_\chi = 0$ and $k_\chi = 3$ within the reaction zone, consistent with the Gaussian pdfs seen in Fig. 9(a). Once again, this is indicative of substantially reduced intermittency in the reaction zone for small I_T.

The insets of the conditional pdfs in Figs. 7 and 8 indicate that the pdfs of $\ln(\Omega)$ and $\ln(\varepsilon^*)$ do not vary much with either Y or I_T, and that the pdfs are negatively skewed compared to Gaussian distributions. The insets in Fig. 9 show, however, that there are large variations in the pdfs of $\ln(\chi)$ with Y and I_T. Figure 11 shows that, in the preheat zone, the conditional skewness, $\tilde{s}_\chi(Y)$, and kurtosis, $\tilde{k}_\chi(Y)$, of $\ln(\chi)$ are only close to the Gaussian values for high I_T (F5). The moments for F1 and F3, by contrast, are substantially different from the Gaussian values in most of the preheat zone. In the reaction zone, significant departures from Gaussianity are observed for all I_T. Variations of the $\ln(\chi)$ moments with Y and I_T in Fig. 11 thus indicate that the log-normal model provides a poor description of the χ statistics in the reaction zone for all I_T, and is only reasonably accurate in the preheat zone for high I_T. As noted in Sec. IV D, the statistics of χ in the reaction zone for low I_T are more accurately described using a Gaussian distribution.

F. Distributions of the internal flame structure

The intermittency of χ is closely connected to the intermittency associated with the local structure of the flame. As discussed in Ref. 22, the internal widths of flamelets within the turbulent flame brush are given by the separation between isosurfaces of Y. Such local widths are connected to χ and are proportional to $\delta_t = (\chi_i \chi_i)^{-1/2}$,[22] where χ_i is the gradient of Y. The true local flame width must also account for the increment in Y and can be written as $\approx \delta_t \Delta Y$. The internal flame structure is broadened relative to the corresponding laminar flame width, $\delta_l(Y)$, if $\delta_t/\delta_l(Y) > 1$. Similarly, the flame is thinned if $\delta_t/\delta_l(Y) < 1$. An analysis of the first-order statistics of δ_t in Ref. 22 has shown that the flame is, for sufficiently high I_T, substantially broadened in the preheat zone. The reaction zone is, however, only slightly broadened, even for the highest value of I_T examined here (F5).

The study of these first-order statistics can be extended by considering distributions of $\delta_t/\delta_l(Y)$ throughout the flame. These distributions are particularly important because locally and instantaneously extreme configurations (e.g., very broad or thin flames) may affect the onset of transient events such as DDT or extinction. Pdfs of $\delta_t/\delta_l(Y)$ in Fig. 12 show that, for all I_T, there is a higher

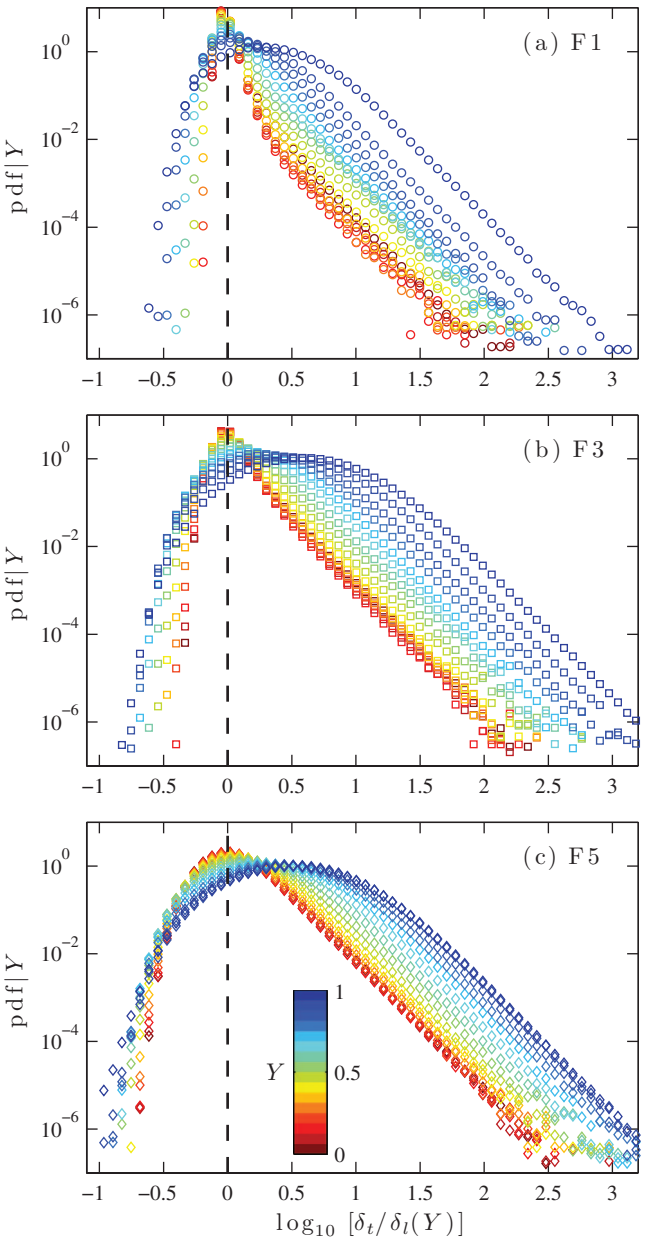

FIG. 12. Conditional pdfs of $\log_{10}[\delta_t/\delta_l(Y)]$ for (a) F1, (b) F3, and (c) F5, where δ_t is the internal width of the turbulent flames and $\delta_l(Y)$ is the corresponding laminar flame width.

probability of obtaining locally broadened flames, as opposed to thinned flames, for all values of Y and I_T. Consistent with prior results in Ref. 22, there is greater flame broadening in the preheat zone than in the reaction zone. Variations in the average flame width are also indicated by Fig. 12; the peaks in the pdfs of $\delta_t/\delta_l(Y)$ shift from large values in the preheat zone (flame broadening) to laminar values in the reaction zone, consistent with prior results.[22]

Variations in the distributions of $\delta_t/\delta_l(Y)$ are connected to changes in the intermittency of χ shown in Figs. 9 and 10. In particular, the intermittency of χ is larger in the preheat zone than in the reaction zone, and the intermittency increases at all Y with increasing I_T. Figure 12 shows that these variations, which are linked to changes in the interactions between turbulence and the flame, have a corresponding effect on the internal structure of the flame.

V. DISCUSSION

As shown in Sec. III, the statistics and intermittency of Ω, ε^*, and ζ in simulations of nonreacting homogeneous isotropic turbulence are consistent with results from prior numerical and experimental studies of a wide range of flows. Statistics from the reacting flow simulations in Sec. IV indicate, however, that there are substantial changes in the intermittency with both turbulence intensity and location in the flame. These changes reflect variations in turbulence-flame interactions with I_T and Y, and also affect the structure and evolution of the flame, as well as the accuracy of the log-normal model in reacting flows.

A. Turbulence intermittency

There are substantial variations in the intermittency of both Ω and ε^* with I_T and location in the flame, as shown in Figs. 7 and 8. For high I_T, the intermittency of Ω and ε^* is relatively unaffected by the flame, which is consistent with prior observations of low-order statistics in premixed reacting flows.[22,52] This invariance is indicated by the similarity of pdfs of Ω and ε^* for all values of Y to the corresponding nonreacting pdfs in Figs. 4(a) and 4(b). For low I_T, however, Ω is more intermittent near the products than the reactants. Consequently, fluctuations about the mean increase from the reactants to the products, even though the mean itself is suppressed in the flame due to dilatational effects from heat release.[22,52–54] The intermittency of ε^* is weaker than that of Ω, and there are also weaker variations in the intermittency of ε^* with both I_T and Y.

These properties of Ω and ε^* can be understood from the interactions between turbulence and flames in premixed reacting flows. It was found in Ref. 22 that for low I_T, the magnitudes of ω_i and S_{ij} (and, by extension, Ω and ε^*) are, on average, suppressed by the flame, and that χ_i has properties similar to those of a laminar flame. For high I_T, however, ω_i and S_{ij} are only weakly affected by the flame, and χ_i begins to resemble a passive scalar gradient. Similar results have also been observed in other studies[55–58] of premixed reacting flows.

Although variations in the mean values of Ω and ε^* are partly responsible for changes to the intermittency, they are not enough to completely explain the dependence of the intermittency on I_T and Y. An additional piece of the puzzle comes from the anisotropic suppression of Ω by the flame, which has been discussed in Ref. 22. The origin of this anisotropic suppression can be understood by decomposing S_{ij} into two components, one due to turbulence and one due to the flame,[22]

$$S_{ij} = S_{ij}^T + n_i n_j S^F, \tag{9}$$

where S_{ij}^T is the turbulent strain rate, $n_i = \chi_i/(\chi_j\chi_j)^{1/2}$ is the local flame direction, and S^F is the strength of the dilatational strain rate imposed by fluid expansion in the flame. Equation (9) is obtained by assuming that the strain rate due to the flame always acts normally to isosurfaces of Y. In Ref. 22, S^F was set equal to the strain produced by a laminar flame corresponding to the parameters in Table I, although for weakly compressible turbulence (as in F1), we can also write $S^F \approx S_{kk}$.

An important consequence of the second term in Eq. (9)—that is, the flame-normal dilatational strain—is that suppression of Ω by the flame is anisotropic. For statistically planar flames, this contributes to a preferred orientation of intense vortical structures perpendicular to the flame front, as observed by Tanahashi *et al.*[59] A mechanism for the creation of this anisotropy was described in Ref. 22, where it was shown that vorticity that is locally oriented in the direction of n_i is relatively unsuppressed by the flame. This can be seen from the transport equation for ω_i, which can be written using Eq. (9) as[22]

$$\frac{D\omega_i}{Dt} \approx \omega_j S_{ij}^T - S_{kk}[\omega_i - (\omega_j n_j)n_i], \tag{10}$$

where $D/Dt \equiv \partial/\partial t + u_j\partial/\partial x_j$, we have used $S^F \approx S_{kk}$, and we have neglected terms due to baroclinic torque and viscous diffusion. The first term on the right side of Eq. (10) represents vortex stretching by the turbulent strain rate, while the second term represents dilatation due to the flame. Multiplying

Eq. (10) by ω_i then gives a transport equation for Ω as

$$\frac{D\Omega}{Dt} \approx \omega_i \omega_j S_{ij}^T - 2\Omega S_{kk}[1 - (\widehat{\omega}_j n_j)^2], \tag{11}$$

where $\widehat{\omega}_i \equiv \omega_i/(\omega_j\omega_j)^{1/2}$ and we assume $\Omega \approx \omega^2/2$. Since the fluid expands through the flame and $S_{kk} > 0$, the last term is typically negative, resulting in a reduction of Ω. When ω_i and n_i are perfectly aligned, however, the second term in Eq. (11) is zero and there is no suppression of Ω from dilatation. The suppression of Ω thus depends on the relative alignment between ω_i and n_i, and is therefore anisotropic.

Anisotropic suppression of Ω may provide an explanation for the variations in turbulence intermittency in premixed reacting flows. In particular, anisotropic suppression allows some vortical structures to pass relatively unsuppressed through the flame, while generally suppressing all other vorticity. This reduces the mean value of Ω in the flame,[22] while also substantially increasing the intermittency due to the presence of some remaining intense structures. These two effects combine to produce strong intermittency in Ω for low I_T within the reaction zone, consistent with the highly stretched pdfs of Ω shown in Fig. 7(a). The intermittency is most pronounced for low I_T and in the reaction zone, and this is where the anisotropic suppression from Eq. (11) is strongest.[22] As I_T increases, anisotropic suppression becomes weaker and the variations in the intermittency through the flame are reduced. The less pronounced variations in the intermittency of ε^* through the flame may be due to the indirect connection between ε^* and vortical structures in turbulent flows. In particular, it was previously observed by Donzis *et al.*[8] that while large values of ε are indeed typically associated with high Ω, intense enstrophy does not always result in intense dissipation. Thus, the anisotropic suppression of Ω has a weaker, less direct effect on distributions of ε^*. The dissipation rate is also affected by fluid expansion in the flame, which introduces a mean velocity gradient $\partial\langle u\rangle_{yz}/dx$ within the flame brush (where $\langle\cdot\rangle_{yz}$ denotes an average over y–z planes). This mean gradient makes no direct contribution to Ω, but may impact distributions of ε^*. It should be noted that anisotropic suppression of Ω may also combine with anisotropic generation by the flame along n_i due to curvature or other effects,[60] and the relative contributions of the suppressing and generating processes deserve further consideration in the future.

The anisotropic suppression explanation for variations in the intermittency of Ω can be tested by integrating a reduced form of Eq. (10). In the limit where S_{ij}^T is small with respect to S^F—which is approximately the case in the reaction zone for low I_T (e.g., F1)—we assume that the first term on the right side of Eq. (10) can be neglected. Also considering a "frozen" vorticity field that does not advect, we obtain a reduced transport equation for ω_i as

$$\frac{d\omega_i}{dt} \approx -S_{kk}[\omega_i - (\omega_j n_j)n_i]. \tag{12}$$

For prescribed S_{kk} and n_i, Eq. (12) can be integrated forward in time given an initial ω_i field. From the resulting evolution of ω_i, pdfs, and hence the intermittency, of Ω can be calculated.

Using this idealized approach, Figure 13 shows that the intermittency of Ω from Eq. (12) increases in time under the influence of anisotropic suppression. In Fig. 13 we use constant S_{kk} and n_i, and use a homogeneous isotropic ω_i field from NR3 as the initial condition. Integration of Eq. (12) is carried out separately at each point in the field. All vorticity not aligned with n_i is suppressed, while initial vorticity aligned with n_i does not change (this can be understood by noting that when $\widehat{\omega}_i n_i = 1$, the right side of Eq. (12) is zero). This gives an increasing suppression of μ_Ω in time, along with an increase in intermittency due to the remaining unsuppressed vorticity.

B. Intermittency in the scalar dissipation rate

Intermittency in χ is connected to the evolution of the flame and distributions of the local flame structure (as discussed in Sec. IV F). Figure 9 shows that, for all I_T, intermittency in χ is greatest near the reactants. For sufficiently high I_T (e.g., F5), there is also significant intermittency near the products. The range of observed χ/μ_χ in Fig. 9 increases with I_T for all Y, consistent with the increase shown in Fig. 4(c) for the simulations of nonreacting passive scalar evolution.

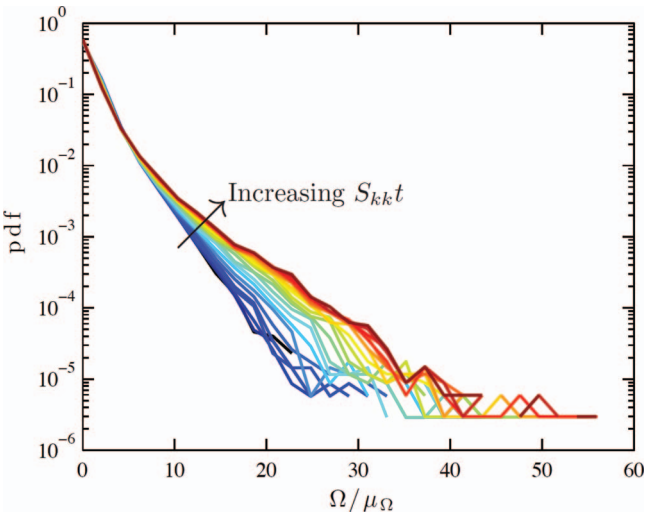

FIG. 13. Time variation of pdfs of Ω/μ_Ω resulting from integration of Eq. (12) using constant n_i and S_{kk}, with an initially homogeneous isotropic vorticity field from NR3. Pdfs are calculated from $S_{kk}t = 0$ (blue) to $S_{kk}t = 2$ (red).

These variations in the intermittency of χ are associated with the balance between production of χ by turbulent straining and reduction of χ by molecular diffusion. When I_T is high, turbulent straining is strong, large values of χ are produced by the turbulence, and the intermittency increases. As I_T decreases, turbulent straining becomes less effective at producing large χ, as compared to reduction by molecular diffusion, resulting in decreased intermittency in both the reacting and nonreacting cases. Variations in the intermittency of χ through the flame can be similarly understood, since dilatation by the flame reduces the strength of turbulent straining, while the strength of molecular diffusion increases due to the increasing temperature. These two effects combine to give weak production of χ, resulting in less intermittent χ fields within the reaction zone, as shown in Fig. 9. The anisotropic suppression of vorticity by the flame may play an additional role in reducing the intermittency of χ in the reaction zone. Vortical structures that are most effective in creating large fluctuations in χ—namely, structures that are perpendicular to the flame normal—are strongly suppressed, while structures that have little effect on χ—those that are parallel to the flame normal—are relatively unsuppressed.

For low I_T, Fig. 9 further shows that pdfs of χ are approximately Gaussian in the reaction zone. For the lowest value of I_T examined here (F1), χ is essentially non-intermittent near the products, but shows significant intermittency near the reactants. These variations are due, in part, to changes with I_T in the scale of the turbulence interacting with the flame. As shown in Ref. 22, the flame suppresses Ω and ε^* (on average) within the reaction zone. This, in turn, suggests that small-scale turbulence is suppressed, since Ω and ε^* are measures of small-scale motions. Consequently, for low I_T, the flame primarily responds only to large-scale turbulent motions within the reaction zone. The large-scale turbulence is approximately Gaussian due to the forcing described in Sec. II, and the fluctuations in χ for low I_T and within the reaction zone may reflect these Gaussian statistics. These results thus suggest that, for low I_T, there may be an imprint of large-scale turbulence on fields of χ. That is, suppression of small-scale turbulence by the flame may expose properties of the large-scale turbulence generation mechanism.

C. Log-normality in reacting flows

The log-normal distribution has been proposed as a model for turbulence intermittency and it has been used to represent the statistics of χ in turbulent combustion models.[36] Figures 7 and 8 show that, as in nonreactive turbulence, the log-normal model (represented by a Gaussian in log coordinates) fails to capture the negative skewness of both $\ln(\Omega)$ and $\ln(\varepsilon^*)$ in premixed

reacting flows. Fluctuations of $\ln(\chi)$ are also negatively skewed, consistent with results from prior studies of various reacting flows.[27–32] Contrary to the statistics of $\ln(\Omega)$ and $\ln(\varepsilon)$, which are only weakly dependent on I_T and Y, the statistics of $\ln(\chi)$—and, hence, the accuracy of the log-normal model—depend on I_T and Y (as shown, for example, in Fig. 11). Consequently, not only does the log-normal model provide a relatively poor approximation for the intermittency of χ, but it also does not predict the dependence of the intermittency on I_T and Y.

Since log-normality is only one of several possible models for turbulence intermittency,[10,26] comparisons with different modeled forms deserve future consideration. The negative skewness of $\ln(\chi)$ shown in Fig. 9 has been observed and discussed in previous studies of scalar dissipation, including in both nonreacting[3,14] and reacting[27–32] flows. Su and Clemens[14] have provided a systematic analysis of the negative skewness, and ultimately conclude that it is a physical feature of pdfs of the scalar dissipation. This skewness has been represented previously[3,27] using exponential distributions for the left tails of the $\ln(\chi)$ pdfs, and examination of these and other distributions is a possible direction for future research. The present results further suggest that improved models for the statistics of χ and $\ln(\chi)$ must additionally include a dependence on I_T and Y.

D. Resolution and Reynolds number effects

As discussed in Sec. III, changing the resolution of the simulations results in changes to the effective Reynolds number. Since intermittency is Reynolds number dependent, we thus expect changes to the measured statistics with varying resolution, even for the same I_T. Despite these expected quantitative changes, however, we can check whether the qualitative trends and insights obtained in the present study are independent of resolution.

We have carried out an additional higher resolution simulation of the intermediate value of I_T examined here (F3). The resolution has been increased by a factor of two in each spatial direction, giving $N_x \times N_y \times N_z = 4096 \times 256 \times 256$ computational grid points. As in the lower resolution simulations, turbulence is allowed to develop for $2\tau_{ed}$ prior to ignition, and the analysis of the data begins another $2\tau_{ed}$ after ignition. The analysis is then carried out over $1.5\tau_{ed}$. Due to the higher resolution and associated computational demands, only one realization of the flow evolution is used in the analysis.

Figure 14 shows pdfs of Ω, ε^*, χ, and the local width $\delta_t/\delta_l(Y)$ through the flame. As in the lower resolution results in Figs. 7(b) and 9(b), the intermittency of Ω and χ varies through the flame, with the greatest intermittency occurring for Ω near the products and for χ near the reactants. Once again, the intermittency of ε^* undergoes weaker changes through the flame. The flame width in Fig. 14(d) is generally broadened, and the extent of broadening is greatest in the preheat zone, consistent with the lower resolution results in Fig. 12(b). The insets of Figs. 14(a)–14(c) show that the disagreement between log-variable pdfs and Gaussian distributions is nearly identical to that found in the lower resolution simulations.

There are quantitative differences between the results in Fig. 14 and Sec. IV due to the varying Reynolds number. In particular, the pdfs of Ω and ε^* are slightly more stretched in the higher resolution simulation as a result of the lower numerical viscosity and, hence, higher effective Reynolds number. The increase in intermittency with Re has also been observed in prior DNS studies.[8] Nevertheless, the results in Fig. 14 show that the qualitative variations of intermittency through the flame are independent of resolution, thus indicating that the lower resolution simulations studied here are sufficient to gain insights into intermittency in premixed reacting flows.

It should be noted that in a realistic premixed reacting flow, the temperature increase from the reactants to products would result in an increase in the physical viscosity and a decrease in the Reynolds number. Since the present study uses numerical viscosity, which is largely temperature independent, this variation of the Reynolds number through the flame and its subsequent effect on the intermittency are not captured. The presence of physical viscosity, however, is likely to have only quantitative, rather than qualitative, effects on the trends presented here. In particular, the change in physical viscosity would act to decrease the mean vorticity of the flow passing through the flame, similar to the effects of fluid expansion by the flame. This change would not affect, however, the anisotropic vorticity suppression discussed in Sec. V A, which is responsible

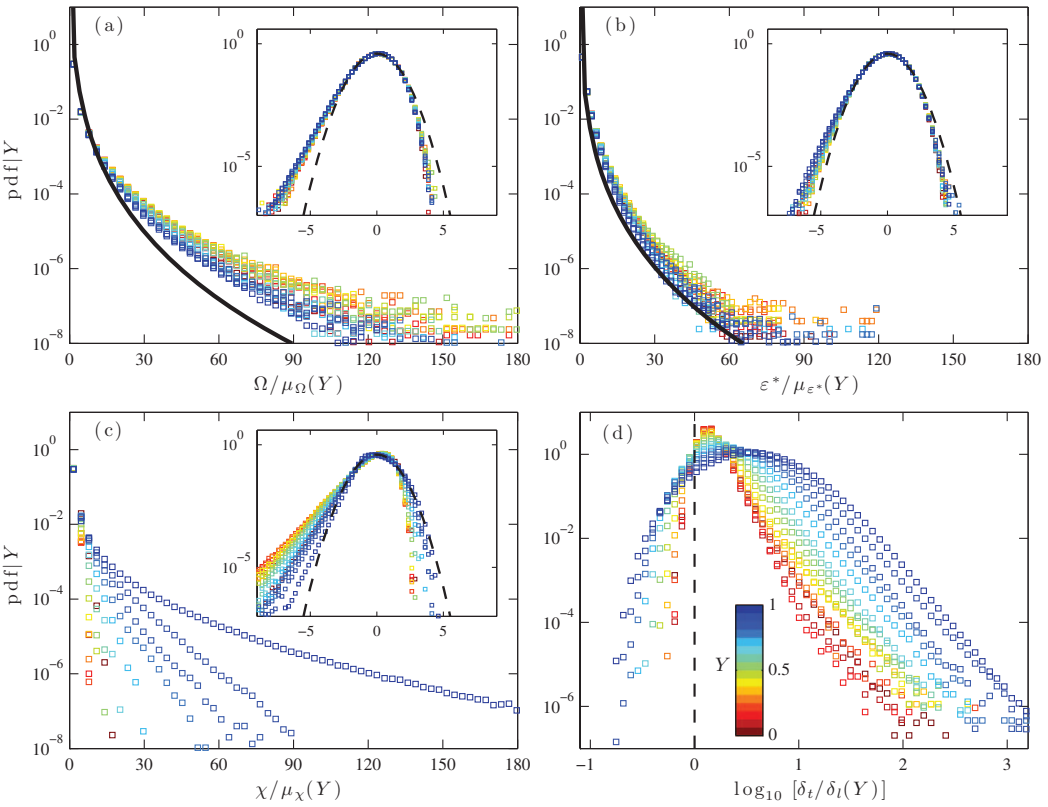

FIG. 14. Conditional pdfs of (a) $\Omega/\mu_\Omega(Y)$, (b) $\varepsilon^*/\mu_{\varepsilon^*}(Y)$, (c) $\chi/\mu_\chi(Y)$, and (d) $\delta_t/\delta_l(Y)$ for the high resolution simulation of F3. Stretched exponentials (black lines) in (a) and (b) are taken from the lower resolution nonreacting results in Figs. 4(a) and 4(b). Insets in (a)–(c) show pdfs of log variables and dashed black lines show Gaussian distributions.

in part for the enhancement of the intermittency associated with Ω and, to a lesser extent, ε^* from the reactants to products. By not including physical viscosity, the effects of fluid expansion and anisotropic vorticity suppression on intermittency can be studied in isolation from changes due to the viscosity. Furthermore, the observed independence of the intermittency of Ω and ε^* on location in the flame at high turbulence intensities would also not be affected by physical viscosity. Once the Kolmogorov scale becomes much smaller than the flame width, the variation in the Kolmogorov scale between reactants and products has only a small dynamical effect. It is nevertheless important, however, to assess in the future the quantitative impact of temperature-dependent physical viscosity on intermittency in reacting flows.

VI. SUMMARY AND CONCLUSIONS

We have studied intermittency in premixed flames by evaluating pdfs and moments of the local enstrophy, Ω, pseudo-energy dissipation rate, ε^*, and scalar dissipation rate, χ. The analysis is based on numerical simulations of statistically planar flames in an unconfined domain at three different turbulence intensities, denoted I_T. The reaction-diffusion model used in the simulations represents stoichiometric H_2-air combustion and the reactants are initially at atmospheric conditions. Simulations of homogeneous isotropic turbulence with a nonreacting and conserved passive scalar have also been carried out in order to validate the numerical method and allow comparisons with the reacting flow results. Statistics from the nonreacting simulations are in close agreement with results from prior numerical[4–9] and experimental[1–3] studies of homogeneous isotropic turbulence and passive scalar evolution. This consistency indicates that the numerical method outlined in

Sec. II is adequate for gaining insights into the intermittency of reacting turbulence using the present simulations.

The reacting flow simulations show that there are substantial changes in the intermittency with both I_T and location in the flame. The latter dependence is studied using conditional statistics based on local, instantaneous values of the reactant mass fraction, Y. For low I_T, the intermittency of Ω varies substantially through the flame, with stronger intermittency near the products. Changes in the intermittency of ε^* are, however, less pronounced. As I_T increases, the intermittencies of both Ω and ε^* become increasingly independent of flame position and are similar to results from the nonreacting simulations. The intermittency of χ is largest near the reactants and increases at all flame locations with increasing I_T. For low I_T, however, pdfs of χ in the reaction zone approximately follow a Gaussian distribution, indicative of substantially reduced intermittency. Deviations from log-normality are observed for all quantities.

Anisotropic suppression of Ω by the flame has been used to explain the increased intermittency of Ω near the products for low I_T. This mechanism suppresses essentially all vorticity except that which is nearly exactly aligned with the direction of the local flame normal. Changes in the intermittency of χ are due to the changing balance between turbulent straining and molecular diffusion with I_T and location in the flame, as well as the suppression of small-scale turbulence by the flame. The latter effect is particularly pronounced in the reaction zone and for low I_T, where the flame interacts primarily with large-scale turbulence. Variations in the intermittency of χ have a corresponding effect on distributions of the local flame structure. In particular, the probability of obtaining broad local flame widths relative to the laminar flame is greatest for high I_T and in the preheat zone at all I_T.

The present study suggests a number of possible directions for future research. Comparisons with the log-normal model suggest that improved models for turbulence intermittency are required in order to accurately predict the occurrence of extreme values of Ω, ε^*, and χ—such extreme values may be important for understanding the onset of DDT, extinction, and re-ignition. The present results further suggest that improved models should take into account variations in the intermittency with I_T and location in the flame. Also, the pdfs of χ for low I_T and in the reaction zone indicate that the large-scale turbulence generation mechanism may affect the intermittency properties of reacting flows. It is thus of interest to consider different turbulence driving mechanisms, for instance involving non-Gaussian distributions and non-Kolmogorov spectra. In order to understand reacting flow intermittency more generally, it is also important to examine how the intermittency changes for different fuel mixtures (such as methane-air) and off-stoichiometric conditions. Finally, insights from the present numerical approach, which uses numerical viscosity, should be examined in the future using calculations with temperature-dependent physical viscosity. This will allow the variations in intermittency observed here to be examined together with variations due to changes in the Reynolds number through the flame.

ACKNOWLEDGMENTS

This work was supported by an award to P.E.H. from the National Research Council Research Associateship Program at the Naval Research Laboratory, by the Air Force Office of Scientific Research Grant No. F1ATA09114G005, and by the Office of Naval Research/Naval Research Laboratory 6.1 Base Program. Computing facilities were provided by the Department of Defense High Performance Computing Modernization Program.

[1] L. K. Su and W. J. A. Dahm, "Scalar imaging velocimetry measurements of the velocity gradient tensor field in turbulent flows. II. Experimental results," Phys. Fluids **8**, 1883–1906 (1996).
[2] B. W. Zeff, D. D. Lanterman, R. McAllister, E. J. Kostellich R. Roy, and D. P. Lathrop, "Measuring intense rotation and dissipation in turbulent flows," Nature (London) **421**, 146–149 (2003).
[3] C. N. Markides and E. Mastorakos, "Measurements of the statistical distribution of the scalar dissipation rate in turbulent axisymmetric plumes," Flow, Turbul. Combust. **81**, 221–234 (2008).
[4] R. S. Miller, F. A. Jaberi, C. K. Madnia, and P. Givi, "The structure and small-scale intermittency of passive scalars in homogeneous turbulence," J. Sci. Comput. **10**, 151–180 (1995).
[5] M. R. Overholt and S. B. Pope, "Direct numerical simulation of a passive scalar with imposed mean gradient in isotropic turbulence," Phys. Fluids **8**(11), 3128–3148 (1996).

[6] P. Vedula, P. K. Yeung, and R. O. Fox, "Dynamics of scalar dissipation in isotropic turbulence: a numerical and modelling study," J. Fluid Mech. **433**, 29–60 (2001).
[7] J. Schumacher, K. R. Sreenivasan, and P. K. Yeung, "Very fine structures in scalar mixing," J. Fluid Mech. **531**, 113–122 (2005).
[8] D. A. Donzis, P. K. Yeung, and K. R. Sreenivasan, "Dissipation and enstrophy in isotropic turbulence: Resolution effects and scaling in direct numerical simulations," Phys. Fluids **20**, 045108 (2008).
[9] D. A. Donzis and P. K. Yeung, "Resolution effects and scaling in numerical simulations of passive scalar mixing in turbulence," Physica D **239**, 1278–1287 (2010).
[10] U. Frisch, *Turbulence: The Legacy of A.N. Kolmogorov* (Cambridge University Press, 1995).
[11] K. R. Sreenivasan, "Possible effects of small-scale intermittency in turbulent reacting flows," Flow, Turbul. Combust. **72**, 115–131 (2004).
[12] P. A. Davidson, *Turbulence: An Introduction for Scientists and Engineers* (Oxford University Press, 2004).
[13] A. Tsinober, *An Informal Conceptual Introduction to Turbulence* (Springer, 2009).
[14] L. K. Su and N. T. Clemens, "The structure of fine-scale scalar mixing in gas-phase planar turbulent jets," J. Fluid Mech. **488**, 1–29 (2003).
[15] T. Boeck, D. Krasnov, and J. Schumacher, "Statistics of velocity gradients in wall-bounded shear flow turbulence," Physica D **239**, 1258–1263 (2010).
[16] P. E. Hamlington, D. Krasnov, T. Boeck, and J. Schumacher, "Statistics of the energy dissipation rate and local enstrophy in turbulent channel flow," Physica D **241**, 169–177 (2012).
[17] G. Samanta, K. D. Housiadas, R. A. Handler, and A. N. Beris, "Effects of viscoelasticity on the probability density functions in turbulent channel flow," Phys. Fluids **21**, 115106 (2009).
[18] P. E. Hamlington, D. Krasnov, T. Boeck, and J. Schumacher, "Local dissipation scales and energy dissipation-rate moments in channel flow," J. Fluid Mech. **701**, 419–429 (2012).
[19] R. W. Bilger, "Some aspects of scalar dissipation," Flow, Turbul. Combust. **72**, 93–114 (2004).
[20] R. W. Bilger, "Turbulent jet diffusion flames," Prog. Energy Combust. Sci. **1**, 87–109 (1976).
[21] K. N. C. Bray, in *Turbulent Reacting Flows*, edited by P. A. Libby and F. A. Williams (Springer-Verlag, New York, 1980).
[22] P. E. Hamlington, A. Y. Poludnenko, and E. S. Oran, "Interactions between turbulence and flames in premixed reacting flows," Phys. Fluids **23**, 125111 (2011).
[23] N. Swaminathan and K. N. C. Bray, "Effect of dilatation on scalar dissipation in turbulent premixed flames," Combust. Flame **143**, 549–565 (2005).
[24] A. Y. Poludnenko and E. S. Oran, "The interaction of high-speed turbulence with flames: Global properties and internal flame structure," Combust. Flame **157**, 995–1011 (2010).
[25] A. R. Kerstein, "Turbulence in combustion processes: modeling challenges," Proc. Combust. Inst. **29**, 1763–1773 (2002).
[26] L. Pan, J. C. Wheeler, and J. Scalo, "The effect of turbulent intermittency on the deflagration to detonation transition in supernova Ia explosions," Astrophys. J. **681**, 470–481 (2008).
[27] A. N. Karpetis and R. S. Barlow, "Measurements of scalar dissipation in a turbulent piloted methane/air jet flame," Proc. Combust. Inst. **29**, 1929–1936 (2002).
[28] E. R. Hawkes, R. Sankaran, J. C. Sutherland, and J. H. Chen, "Scalar mixing in direct numerical simulations of temporally evolving plane jet flames with skeletal CO/H_2 kinetics," Proc. Combust. Inst. **31**, 1633–1640 (2007).
[29] D. O. Lignell, J. H. Chen, and H. A. Schmutz, "Effects of Damköhler number on flame extinction and reignition in turbulent non-premixed flames using DNS," Combust. Flame **158**, 949–963 (2011).
[30] C. Pantano, S. Sarkar, and F. Williams, "Mixing of a conserved scalar in a turbulent reacting shear layer," J. Fluid Mech. **481**, 291–328 (2003).
[31] S. H. Starner, R. W. Bilger, M. B. Long, J. H. Frank, and D. F. Marran, "Scalar dissipation measurements in turbulent jet diffusion flames of air diluted methane and hydrogen," Combust. Sci. Tech. **129**, 141–163 (1997).
[32] Y.-C. Chen and M. Mansour, "Measurements of scalar dissipation in turbulent hydrogen diffusion flames and some implications on combustion modeling," Combust. Sci. Tech. **126**, 291–313 (1997).
[33] A. M. Oboukhov, "Some specific features of atmospheric turbulence," J. Fluid Mech. **13**, 77–81 (1962).
[34] A. N. Kolmogorov, "A refinement of previous hypotheses concerning the local structure of turbulence of a viscous incompressible fluid at high Reynolds number," J. Fluid Mech. **13**, 82–85 (1962).
[35] S. B. Pope, *Turbulent Flows* (Cambridge University Press, 2000).
[36] T. Poinsot and D. Veynante, *Theoretical and Numerical Combustion* (Edwards, 2005).
[37] E. Effelsberg and N. Peters, "Scalar dissipation rates in turbulent jets and jet diffusion flames," Symp. (Int.) Combust. **22**(1), 693–700 (1989).
[38] M. R. Overholt and S. B. Pope, "Direct numerical simulation of a statistically stationary, turbulent reacting flow," Combust. Theor. Model. **3**, 371–408 (1999).
[39] V. N. Gamezo, T. Ogawa, and E. S. Oran, "Flame acceleration and DDT in channels with obstacles: effect of obstacle spacing," Combust. Flame **155**, 302–315 (2008).
[40] P. E. Hamlington, A. Y. Poludnenko, and E. S. Oran, "Turbulence and scalar gradient dyanmics in premixed reacting flows," AIAA Paper, 2010–5027, 2010.
[41] P. E. Hamlington, A. Y. Poludnenko, and E. S. Oran, "Intermittency and premixed turbulent reacting flows," AIAA Paper 2011–113, 2011.
[42] A. Y. Poludnenko and E. S. Oran, "The interaction of high-speed turbulence with flames: turbulent flame speed," Combust. Flame **158**, 301–326 (2011).
[43] T. A. Gardiner and J. M. Stone, "An unsplit Godunov method for ideal MHD via constrained transport in three dimensions," J. Comp. Phys. **227**, 4123–4141 (2008).

[44] P. Colella, "Multidimensional upwind methods for hyperbolic conservation-laws," J. Comp. Physiol. **87**, 171–200 (1990).
[45] J. Saltzman, "An unsplit 3D upwind method for hyperbolic conservation-laws," J. Comp. Physiol. **115**, 153–168 (1994).
[46] N. Peters, *Turbulent Combustion* (Cambridge, 2000).
[47] J. P. Boris, in *Whither Turbulence? Turbulence at the Crossroads*, edited by J. L. Lumley (Springer-Verlag, New York, 1990).
[48] W. J. Rider, F. F. Grinstein, and L. G. Margolin, *Implicit Large Eddy Simulation* (Cambridge University Press, 2007).
[49] R. Benzi, L. Biferale, R. T. Fisher, L. P. Kadanoff, D. Q. Lamb, and F. Toschi, "Intermittency and universality in fully developed inviscid and weakly compressible turbulent flows," Phys. Rev. Lett. **100**, 234503 (2008).
[50] D. Porter, A. Pouquet, and P. Woodward, "Measures of intermittency in driven supersonic flows," Phys. Rev. E **66**, 026301 (2002).
[51] H. Tennekes, "Intermittency of the small-scale structure of atmospheric turbulence," Boundary Layer Meteorol. **4**, 241–250 (1973).
[52] C. J. Mueller, J. F. Driscoll, D. L. Reuss, M. C. Drake, and M. E. Rosalik, "Vorticity generation and attenuation as vortices convect through a premixed flame," Combust. Flame **112**, 342–358 (1998).
[53] P. A. McMurtry, J. J. Riley, and R. W. Metcalfe, "Effects of heat release on the large-scale structure in turbulent mixing layers," J. Fluid Mech. **199**, 297–332 (1989).
[54] A. N. Lipatnikov and J. Chomiak, "Effects of premixed flames on turbulence and turbulence scalar transport," Prog. Energy Combust. Sci. **36**, 1–202 (2010).
[55] N. Swaminathan and R. W. Grout, "Interaction of turbulence and scalar fields in premixed flames," Phys. Fluids **18**, 045102 (2006).
[56] S. H. Kim and H. Pitsch, "Scalar gradient and small-scale structure in turbulent premixed combustion," Phys. Fluids **19**, 115104 (2007).
[57] N. Chakraborty and N. Swaminathan, "Influence of the Damköhler number on turbulence-scalar interaction in premixed flames. I. Physical insight," Phys. Fluids **19**, 045103 (2007).
[58] G. Hartung, J. Hult, C. F. Kaminski, J. W. Rogerson, and N. Swaminathan, "Effect of heat release on turbulence and scalar-turbulence interaction in premixed combustion," Phys. Fluids **20**, 035110 (2008).
[59] M. Tanahashi, M. Fujimura, and T. Miyauchi, "Coherent fine-scale eddies in turbulent premixed flames," Proc. Combust. Inst. **28**, 529–535 (2000).
[60] A. B. Zel'Dovich, A. G. Istratov, N. I. Kidin, and V. B. Librovich, "Flame propagation in tubes: Hydrodynamics and stability," Comb. Sci. Tech. **24**, 1–13 (1980).